International Journal of Engineering Research and Development
e-ISSN: 2278-067X, p-ISSN: 2278-800X, www.ijerd.com
Volume 13, Issue 43 (April 2017), PP.32-57

Review and Assessment of Turbulence Transition Models

Gary C. Cheng[1], Robert Nichols[2], Kshitij D. Neroorkar[3]
[1]*University of Alabama, Associate Professor, Aerospace Engineering and Mechanics Department, Tuscaloosa, USA.*
[2]*University of Alabama at Birmingham, Research Professor, Mechanical Engineering Department, Birmingham, AL 35294-4461, UAS.*
[3]*CD-Adapco, Development Engineer, Bangalore, India .*

***ABSTRACT*:** Turbulent boundary layer transition can greatly affect flow characteristics such as skin friction, heat transfer, pressure loads, and boundary layer separation point. Accurate computation of such effect is vital to the design of components and vehicles subjected to turbulent transition flows. In this paper we report our review of the existing boundary layer transition models, selection of the boundary layer transition models most appropriate for the existing Reynolds-averaged Navier-Stokes flow solvers, and implementation and evaluation of the selected transition models with some benchmark test cases, ranging from subsonic to hypersonic flows. The objective of this assessment study is not intended to pick the best transition model (in fact, there is no transition model accurately predict the boundary layer transition for all cases tested here). Rather it is to demonstrate that (1) the flow physics of turbulence transition is very complicated and not yet well understood, (2) the applicability of empirical transition models is limited and their use should be cautious due to different transition characteristics for different flow regimes/environments, and (3) further research on prediction of turbulence transition is warranted to improve the accuracy, efficiency and range of applicability.

Keywords:- Turbulence models, turbulence transition, CFD, flat plate, hypersonic cylindrical cone, turbine cascade.

I. INTRODUCTION

The transition of a boundary layer from laminar to turbulent has been found to impact the characteristics of a flow field, but its underlying physics has yet to be well understood. The lack of boundary layer transition simulation is a major source of error for many applications, such as Reynolds number scaling of wind tunnel results to flight, hypersonic flight, and high altitude turbine engine propulsion. In spite of the large amount of turbulence transition data available, no empirical method has been formulated that can reliably predict transition for a variety of flight conditions and geometries. Though current efforts using Direct Numerical Simulations are interesting and have shown promising results, their use in production applications on real geometries is years away. Another method that has been investigated is the use of the boundary layer stability theory. This method has a number of shortcomings, and the most significant of these are (1) they cannot be used for simulating bypass transition, and (2) they can be only used to predict the onset of transition and not for modeling the region itself. Probably the most popular method for modeling transition is the use of low Reynolds number Reynolds-Averaged Navier-Stokes (RANS) codes, either directly or in conjunction with some empirical correlations to facilitate transition modeling. The use of low Reynolds number RANS models has proven unreliable in predicting the change in skin friction and heat transfer within the transition region. No model of this type performs satisfactorily under the influence of freestream turbulence intensity and pressure gradients. It is extremely difficult to obtain the correct location of the onset of transition with this class of models. Recently methods have been developed for simulating boundary layer transition, which solve transport equations for intermittency or for a disturbance kinetic energy. These models rely heavily on empirical functions to predict the onset and extent of the transition region. Transport based transition models are of current interest because they can be easily coupled to existing transport equation turbulence models and can be used on complex configurations. Unfortunately the existing transition models were tuned and validated for a limited number of test cases. Hence it is valuable to have a third-party evaluation of the transition models currently available using benchmark test cases for subsonic to hypersonic flows in order assess the accuracy and range of these new models. It is hoped to either extend their applicability range or to possibly dismiss them entirely as a viable tool.

In the present study the investigators have (1) performed literature review of both numerical and experimental studies of turbulence transition flows, (2) selected turbulence transition models suitable for the existing RANS flow solvers, (3) selected benchmark test data for validating and evaluating turbulence transition models, and (4) modified existing RANS CFD codes to include the selected transition models for assessment.

The results from this assessment study can provide users with an "honest broker" evaluation of current turbulence transition models.

II. LITERATURE REVIEW

Turbulence transition models have been broadly categorized in two groups: models based on stability theory and models not based on stability theory. Models not based on stability theory are further divided into two groups: models with known transition onset and models with onset prediction capability.

A. Models Based on Stability Theory

The e^n method proposed by Smith and Gamberoni [1] and Van Ingen [2] is based on the linear stability theory and is one of the most popular methods available for transition prediction. There are three steps in the application of the e^n method: (1) computing the laminar velocity and temperature profiles at different streamwise locations for the given flow; (2) calculating the amplification rates of the most unstable waves for each profile by using the e^n method; (3) calculating the transition location using these amplification rates. There are several problems associated with the e^n method. The major criticism that the e^n method has received is that it was developed based on the linear stability theory with an assumption that the flow is locally parallel. The value of the '*n*' factor for transition is not universal and needs to be determined based on experimental data. This value varies from one wind tunnel to the next.

The linear Parabolized Stability Equations (PSE) method addresses the non-parallel effects neglected in the linear stability theory and assumes that the mean flow, amplitude functions and wave number are dependent upon the streamwise distance. A further development of the linear PSE, known as the nonlinear PSE, incorporates the nonlinear effects that have been neglected in the linear stability theory. Methods based on the stability theory have one major drawback - they need to track the growth of the disturbance amplitude along a streamline. This limitation poses a significant problem for three-dimensional flow simulations where the streamline direction is not aligned with the grid. Coupling of such methods with CFD codes requires an unrealistically high grid density to yield the boundary layer data with the required level of accuracy. These methods also require a well-converged steady-state solution, which may not be obtainable for real-world problems involving local flow separation. The main advantage of these methods is that they give the correct treatment of the surface curvature. Some different techniques have been employed to use these stability-based methods more efficiently [3]. One method is to generate a database of the solution of the linear stability equation for different velocity profiles in advance. The local flow stability can then be determined quickly based on the local velocity calculated from CFD codes. The validity of these models is limited to the range of velocity profiles available in the database.

B. Models not Based on Stability Theory

1) Models with Known Transition Onset:

The transition models in this group are unable to predict the location of the transition. The transition location is determined from empirical data or results from an e^n computation. The transition region is modeled by modifying existing turbulence models. In [4], six transition models were implemented into the commercial Navier-Stokes code-- GASP. These six models were the Baldwin-Lomax model; the Wilcox k-ω model; the Schmidt and Patankar low-Re k-ε model that had a production term modified for modeling transition; the Warren, Harris and Hasan one-equation model; the algebraic transition model developed at ONERA/CERT; and, finally, the linear combination transition model developed by Dey and Narasimha. These models were used to simulate hypersonic experimental cases that included transition on a cone at Mach 6 [5], a compression ramp at Mach 10.08 [6], and five flared cone test cases at Mach 7.93 [7], [8]. Out of the five flared cones used there were two with favorable pressure gradients, two with adverse gradients, and one with a zero pressure gradient.

In [4], the Baldwin-Lomax algebraic turbulence model was used to predict the transition region by turning off the turbulence model (setting the eddy viscosity equal to zero) for the laminar flow region, and allowing the turbulence model to produce eddy viscosity beginning at the transition point. It was found that in most of the cases this model adequately predicted the peak heat transfer, but under predicted the transition length [4]. Warren, Harris and Hassan (WHH) [9] proposed a one-equation model to include the effect of second mode disturbances in addition to the first mode. The transitional stress, incorporating both modes, is calculated using an empirical correlation. The equation for calculating the intermittency factor was developed by Dhawan and Narasimha [10]. The applicability of this equation has been confirmed for hypersonic flows. In [9], the model was used to simulate cases in which the first mode disturbances dominate the transition process ($M < 4$) and cases in which the second modes are dominant ($M > 4$). In all cases, the model performed satisfactorily. This model was later implemented in [4] and again was found to be quite accurate. The low-Re k-ω model developed by Wilcox [11]-[12] was used to predict the transition region in [4]. The prediction of the transition region was obtained by tripping the boundary layer at a given point by decreasing the value of the

dissipation so as to destabilize the boundary layer and cause transition. The application of this model in [4] showed that it was not very easy to trip the boundary layer at the desired location due to the sensitivity to the initial conditions. This model predicted a short transition length and over-predicted the peak heat transfer for some cases. Schmidt and Patankar [13] have developed modifications to the production term in the turbulent kinetic energy (TKE) equation of the Lam and Bremhorst k-ε model [14]. These modifications limited the production of the kinetic energy. For the use of this model, a trial and error method was needed to make transition occur at the desired position by varying the inlet conditions. The results did not compare well to the experimental cases in [4], and the method was found to be very sensitive to the grid spacing near the wall. Due to the defects in this model a few modifications were suggested in [4]. Since it was found that the model had difficulty triggering turbulence transition, a spot with high TKE was introduced into the boundary layer. This spot then grew and caused transition to take place. In order to improve the prediction of the length of the transition region, an exponential function was used for the maximum allowable production of TKE. These modifications improved the results for some cases but gave worse results for other cases. An algebraic transition model was developed at ONERA/CERT and is described in Arnal [15]-[16]. The form of the model in Singer *et al*. [17]-[18] was implemented in [4]. This model predicts transition by multiplying the eddy viscosity by a transition function before adding it to the fluid viscosity. This transition function was found to be related to the momentum thickness growth. As a result, in test cases with severe adverse pressure gradients, where the momentum thickness decreases, the model did not produce transition. Theoretically this model should be compatible with any turbulence model. However, it was found that this model did not perform well with two-equation models. In [4], the model was used with the Baldwin-Lomax model. Corrections to the calibration of the transition function for high speed flows were also suggested in [4]. The new model predicted the cases tested in [4] better than the original model. Dey and Narasimha [19] developed a linear combination transition model based on the concept that the transition flow is a combination of the laminar and turbulent flow fields. The contribution from laminar and turbulent values is proportioned based on the intermittency factor developed by Dhawan and Narasimha [10] mentioned above. This model requires that a complete laminar flow simulation be run first, which is followed by a turbulent one, with the turbulent boundary layer starting at the point of transition. The model then uses these two solutions to generate the transitional solution. The main difficulty in getting accurate results with this model was that one of the modeling constants needs to be modified from case to case to obtain good results. Many researchers such as Abid [20] have used the intermittency function from the linear combination model as an algebraic transition region function to proportion the amount of the eddy viscosity added to the fluid viscosity. The results using this method were found to be very similar to the linear combination model mentioned above, but there are some noticeable differences [4]. The transition length was always under-predicted. For the cases with no pressure gradient and adverse pressure gradients, the heat transfer predicted at the end of transition and through the turbulent region was significantly high.

In addition to the above models, there have been several efforts to modify existing turbulence models for turbulence transition. In [21], the performance of the Spalart-Allmaras (S-A) [22] and the Baldwin-Barth (B-B) [23] one-equation models and three two-equation models for simulating hypersonic transition were evaluated. The two-equation models assessed in [21] included a low-Re k-ε model with the modifications of Nagano and Hishida [24], the hybrid k-ω model of Menter [25], and the Wilcox k-ω model [26]. The Sandia Advanced Code for Compressible Aerothermodynamics Research and Analysis (SACCARA) was used to evaluate these models in [21] using two flow cases. The first case was the flow over a flat plate at Mach 8 with flow conditions corresponding to an altitude of 15 km, where a perfect gas was assumed. The second flow case considered was the flow over a re-entry flight vehicle at Mach 20 and an altitude of 24.4 km, where real gas effects need to be included. In the method employed in [21] the turbulence transport equations were solved over the entire domain, with a transition plane specified by the user. Upstream of this plane, the effective viscosity was simply the laminar value, whereas at downstream the effective viscosity was the sum of the laminar and turbulent viscosities. An advantage of this approach was that the turbulence transport equations were solved over the whole domain, thus promoting turbulent behavior downstream of the transition plane. On the other hand, if the turbulence source terms were simply turned on after the transition plane, the turbulence model might not transition to turbulent flow until farther downstream, depending on the freestream turbulence level. A disadvantage of the approach was that a discontinuity in the total viscosity (laminar plus turbulent) could occur at the transition plane. All models, except the S-A model and the low-Re k-ε model, predicted the transition at the correct location for the flat plate case at Mach 8. For these two models, the freestream turbulence values needed to be increased. All the models tested in [21] provided the correct skin friction levels for this case. For the reentry flight vehicle, the wall heat flux predicted by the S-A model, the Menter k-ω model, and the Wilcox k-ω model were found to be in reasonable agreement with the experimental data. The B-B and the low-Re k-ε model greatly over-predicted the heat flux in the turbulent region.

2) Models with Onset Prediction Capability:

This family of models not only simulates the characteristic of the transition region, but also predicts the onset of transition.

The k-ζ turbulence model [27] was used to study the effect of high disturbance environments (HIDE) on turbulence transition occurred in conventional hypersonic facilities. Since HIDE cannot be described by linear stability theory, a minimum heat flux criterion was used to determine onset of transition. This is done by assuming initial transition onset points and employing linear interpolation for interior points. After running a few iterations, a criterion is employed to find the locations of the minimum wall heat flux. The solution is independent of the initial guess as long as the initial transition points are ahead of the actual locations. This approach is similar to the WHH model mentioned above. The dissipation time scale in the turbulent kinetic energy equation was also chosen as the combination of time scales of turbulent and non-turbulent fluctuations. The time scale for calculating the eddy viscosity and the dissipation time scale were derived for three different transition mechanisms: crossflow instabilities, second mode instabilities, and HIDE. These three mechanisms were selected because they were believed to be responsible for transition over 3-D bodies in conventional hypersonic wind tunnels [28]. The simulations were performed on an elliptic cone at the Mach number of 7.93 and were compared with experimental results. It was concluded from the results that HIDE had a higher impact on the transition mechanism than the other two mechanisms. The main disadvantage of this model is that it does not solve the non-turbulent fluctuations using transport equations, which limits the flexibility of this method. Also, this model requires an initial guess for the transition location.

Papp and Dash model [29] employed a concept analogous to that of the WHH model. In this model, a so-called SSGZ-J k-ε model developed by So *et al*. [30] was implemented with compressibility corrections for hypersonic flows. An additional transport equation was solved for the non-turbulent fluctuations. The non-turbulent fluctuations included the first- and second-mode mechanisms. This equation is of the similar form as the turbulent kinetic energy equation of the SSGZ-J model. In this case, the transition onset was determined by a minimum skin friction criterion mentioned in [31], which is an alternative to the e^n method. The location of the transition onset was said to be the minimum distance along the surface for a transition onset parameter to be greater than 1. The laminar turbulent kinetic energy is calculated from a transport equation in the Papp and Dash model [29]. This model was incorporated into a RANS flow solver by multiplying the turbulent eddy viscosity with the intermittency before adding it to the fluid viscosity. In all cases simulated, the transition onset was properly obtained. However, in some cases the peak in heat transfer was not reproduced correctly. This has been attributed to the algebraic nature of the intermittency function used. This is the biggest disadvantage of the model.

Suzen and Huang [32] used a transport equation for the intermittency factor. This equation not only reproduces the intermittency distribution of Dhawan and Narasimha [10], but also gives a realistic variation of the intermittency in the cross-stream direction. The intermittency transport equation includes source terms from two different models: the Steelant and Dick model [33] and the Cho and Chung model [34]. The model is incorporated into a RANS solver by simply multiplying the eddy viscosity obtained from Menter's shear stress transport (SST) model [25] with the intermittency factor. The onset of transition was determined by comparing the local Reynolds number with a transition onset Reynolds number (Re_θ) calculated using the correlation of Huang and Xiong [35], where Re_θ is a function of the freestream turbulent intensity and the acceleration parameter. This model was tested for zero-pressure and variable-pressure gradient flows with different freestream turbulence intensities. The numerical result showed good agreement with the experimental data of Savill [36] and [37]. This model is not a single point model since it uses the freestream turbulence intensity value to calculate the transition onset Reynolds number, which requires global parameters.

Walters and Leylek model [38] was developed based on the concept that bypass transition is caused by very high amplitude streamwise fluctuations. These fluctuations are very different from turbulent fluctuations. Mayle and Schulz [39] proposed a second kinetic energy equation to describe these fluctuations. This kinetic energy was called laminar kinetic energy k_L. In the near-wall region, the turbulent kinetic energy (TKE, k_T) was split into small-scale energy and large-scale energy. The small-scale energy ($k_{T,s}$) contributes directly to the turbulence production, and the large-scale energy ($k_{T,l}$) contributes to the production of laminar kinetic energy. These two energies can be calculated from k_T based on the turbulent length scale. The eddy viscosities based on both scales are calculated from the respective-scale turbulent kinetic energies. For the onset of transition, a parameter is calculated from k_T, the kinematic viscosity and the wall distance. When this parameter exceeds a certain threshold, transition is assumed to start. The onset of transition is associated with the reduction of k_L and the consequent increase of k_T (indicating the breakdown of laminar fluctuations into turbulence). This model was incorporated into a RANS flow solver for the calculation of the total eddy viscosity and eddy thermal diffusivity to account for contributions from the small-scale and large-scale turbulent kinetic energies. For all test cases simulated, the model responded correctly to increases in the freestream intensity. It yielded

reasonable results for cases with high pressure gradients and streamline curvatures. Advantages of this method are that it is very simple to implement it into the existing RANS-based CFD codes. This is a single point transition model meaning that it requires only local information, which makes this method easily applicable to unstructured and parallel computations. The low-Re k-ε models are typically not calibrated for transition prediction, but provide the transition location as a by-product of their viscous sublayer formulation. Since this transition model is developed based on the low-Re k-ε model, the embedded viscous sublayer formulation coupled with the added transition prediction capability cannot be calibrated independently. Hence, a change in the transition formulation would affect the solution in the fully turbulent region. In addition, it is generally observed that these models are not flexible enough to sufficiently cover the wide range of transition mechanisms [40]-[41].

The Local Correlation Based Transition Model (γ-Re_θ model or LCTM) [40]-[41] employed an important parameter, vorticity Reynolds number, which is a local property and can be easily calculated in CFD codes. The maximum value of the vorticity Reynolds number in a boundary layer profile is directly proportional to the momentum thickness Reynolds number. The vorticity Reynolds number is used in triggering transition instead of directly using the momentum thickness Reynolds number. This model solves a transport equation for intermittency and also a transport equation for the Reynolds number based on the transition onset momentum thickness $(\overline{\mathrm{Re}_{\theta t}})$. The first transport equation includes two terms that control production. These are F_{length}, a parameter controls the length of transition zone, and $\mathrm{Re}_{\theta c}$ which is the momentum thickness Reynolds number at the point where the intermittency starts to increase in the boundary layer. These two variables are calculated from empirical functions of $\mathrm{Re}_{\theta t}$. The second transport equation is required to include the non-local influence of the turbulence intensity, which varies with the freestream turbulent kinetic energy and the freestream velocity. In the case of flows with boundary layer separation, this transition model is modified so that the intermittency is allowed to exceed the unity when the boundary layer separates. This event results in larger production of kinetic energy leading to correct prediction of reattachment [41]. This model is applied by modifying the production and destruction terms of the original SST model using the intermittency. The model was validated with some complicated 2D and 3D configurations. In all cases, good agreement with the experimental data was obtained. This model offers two main advantages: (1) it is based on local variables; (2) it is very flexible and can be used for any transition mechanism. However, the empirical correlations used with this model are proprietary.

The transition model by Lodefier *et al*. [42] is also based on the concept of pre-transitional fluctuations similar to the Walters and Leylek model. However, this model uses the concept of intermittency to describe the transition region. The intermittency equation used in this model was proposed by Steelant and Dick [43]. The production term of this intermittency equation was modified by multiplying intermittency with a new factor which is used to locate the start of transition. This factor is zero before the start of transition and rapidly goes to unity after the onset point. Similar to LCTM, the vorticity Reynolds number is used in triggering transition instead of directly using the momentum thickness Reynolds number ($\mathrm{Re}_{\theta t}$). Unlike LCTM, the equation used to calculate the critical value of $\mathrm{Re}_{\theta t}$ for transition is calculated from the local freestream turbulence intensity and not from a transport equation. The employed empirical correlation for $\mathrm{Re}_{\theta t}$ does not include a pressure gradient term. The model is incorporated into the SST model both by multiplying the eddy viscosity with the intermittency and by modifying the production terms of the k and ω equations. These modifications are used to ensure that the turbulence quantities have small nonzero values at the start of transition as in the concept of pre-transitional fluctuations. The main disadvantage of this model is that it uses the freestream intensity to determine the onset of transition, which makes the model non-local unlike LCTM.

Lian and Shyy [44] developed a transition model for simulation of flow around the wing of a micro air vehicle. The approach used in this model was to couple an incompressible RANS solver with the e^n method. The k-ω model of Wilcox [11] was selected for modeling turbulence in the RANS solver. This coupling is accomplished as follows. The computation is started with the solution of the RANS equations; however, the eddy viscosity is not added to the effective viscosity. The boundary layer parameters required for the solution of the e^n method are extracted from the Navier-Stokes solutions to evaluate the amplification factor. Once the threshold value of the n-factor is reached, the flow is allowed to become turbulent by multiplying the eddy viscosity with the intermittency factor and adding it to the effective viscosity. The intermittency in this case is calculated from an empirical formula. The e^n method employed is based on the assumptions of small initial disturbance and thin boundary layer.

The model by Arthur and Atkin [3] is based on the linear stability theory (e^n method) within a RANS framework. The overall process is as follows. The viscous flow over the configuration of interest is first calculated with an initial guess of the transition onset location. A series of pressure distributions is extracted from the RANS solution at different "line- of-sight" positions across the span. These pressure distributions are fed into a boundary layer code to predict the boundary layer parameters. The stability analysis, together with

some "*n*" factor criterion is conducted to yield the transition location. This information is then passed onto the RANS solver for further solution. This process is continued until the transition location and the pressure distribution are converged. For flows with high pressure gradients, it was found that the predicted transition location can move upstream more easily than downstream during the iteration process. Thus, for this method it is essential that the initial guess is downstream of the final, predicted transition location. The method does not have any intermittency model to predict the nature of the transition region.

Based on the literature survey, it is concluded that LCTM [40]-[41] and the Walters and Leylek model [38] constitute the formulations best suited for production CFD codes because they are both single-point models that can be easily incorporated into the existing RANS CFD codes. Both of these models provide an estimate of the location for turbulence transition and enable the CFD codes to simulate the flow characteristics in the transition region. These two models have been found to produce transition locations that respond properly to changes in freestream turbulence intensity and local pressure gradients.

III. FORMULATION OF SELECTED TURBULENCE TRANSITION MODELS

A. Walter-Leylek Model [38]:

The Walters-Leylek model is built based on the low-Re k-ε mode. To illustrate the difference the low-Re k-ε model is included here. For the low-Re k-ε model the eddy viscosity models can be expressed as

$$-\overline{\rho u_i u_j} = 2\mu_T S_{ij} - \frac{2}{3}k_T\delta_{ij} \quad ; \quad S_{ij} = \left(\frac{\partial U_i}{\partial X_j} + \frac{\partial U_j}{\partial X_i}\right) \tag{1}$$

$$-\overline{\rho u_i \theta} = \alpha_{\theta,T}\frac{\partial \theta}{\partial X_i} \tag{2}$$

where U_i and θ are the mean velocity components and mean temperature, and k_T, μ_T and $\alpha_{\theta,T}$ are the turbulent kinetic energy, eddy viscosity and eddy thermal diffusivity, respectively. μ_T and $\alpha_{\theta,T}$ are formulated as

$$\nu_T = \frac{\mu_T}{\rho} = C_\mu \frac{k_T^2}{\varepsilon} \quad ; \quad \alpha_{\theta,T} = \frac{\mu_T}{\mathrm{Pr}_T} \quad ; \quad S^2 = 2S_{ij}S_{ij} \tag{3}$$

where Pr_T is the turbulent Prandtl number. In the Walters-Leylek model, the transport equation of the turbulent kinetic energy is modified as

$$\frac{D\rho k_T}{Dt} = \rho P_T + \frac{\partial}{\partial X_j}\left[\left(\mu + \frac{\alpha_T}{\sigma_k}\right)\frac{\partial k_T}{\partial X_j}\right] - \rho\varepsilon + \rho R + \rho R_{NAT} - D_T \tag{4}$$

where P_T is production of turbulence by turbulent fluctuation, R is production of turbulence by laminar fluctuation, R_{NAT} is production of turbulence due to flow instabilities, and D_T is the near-wall dissipation of turbulence. R_{NAT} may be neglected if the effect of natural transition will not be included. These terms will be described in the following:

where k_L is the laminar kinetic energy due to flow fluctuation, and d is the normal distance away from the wall.

$$\begin{gathered} P_T = \nu_{T,s} S^2 \quad ; \quad \nu_{T,s} = f_v f_{\tau,s} C_{\mu,s}\sqrt{k_{T,s}}\,\lambda_{\mathrm{eff}} \quad ; \quad \lambda_{\mathrm{eff}} = \mathrm{Min}\{C_\lambda d, \lambda_T\} \quad ; \quad \lambda_T = k_T^{1.5}/\varepsilon \\ k_{T,s} = k_T\left(\frac{\lambda_{\mathrm{eff}}}{\lambda_T}\right)^{2/3} \quad ; \quad f_v = 1 - e^{-\sqrt{\mathrm{Re}_{T,s}}/A_v} \quad ; \quad f_{\tau,s} = 1 - e^{-C_{\tau,s}(\tau_m/\tau_{T,s})^2} \quad ; \quad \mathrm{Re}_{T,s} = \frac{k_T^2}{\nu\varepsilon} \\ C_{\mu,s} = \frac{1}{A_0 + A_s\left(\frac{Sk_T}{\varepsilon}\right)} \quad ; \quad \tau_m = \frac{1}{S} \quad ; \quad \tau_{T,s} = \frac{\lambda_{\mathrm{eff}}}{\sqrt{k_{T,s}}} \quad ; \quad \alpha_T = \rho f_v C_\mu \sqrt{k_{T,s}}\,\lambda_{\mathrm{eff}} \end{gathered} \tag{5}$$

$$R = C_R \beta_{BP}\frac{k_L}{\tau_T} \quad ; \quad \tau_T = \frac{\lambda_{\mathrm{eff}}}{\sqrt{k_T}} \quad ; \quad \beta_{BP} = 1 - e^{\frac{-\phi_{BP}}{A_{BP}}} \quad ; \quad \phi_{BP} = \mathrm{Max}\left\{\left(\frac{\sqrt{k_T}\,d}{\nu} - C_{BP,Crit}\right), 0\right\} \tag{6}$$

$$\begin{gathered} R_{NAT} = C_{R,NAT}\beta_{NAT}k_L S \quad ; \quad \beta_{NAT} = 1 - e^{-B_{NAT}/A_{NAT}} \\ B_{NAT} = \mathrm{Max}\left\{\left(\phi_{NAT}^{0.75}\phi_{MIX}^{0.25} - C_{NAT,Crit}\right), 0\right\} \quad ; \quad \phi_{NAT} = \frac{d^2 S}{\nu} \quad ; \quad \phi_{MIX} = \frac{\sqrt{k_L}\,d}{\nu} \end{gathered} \tag{7}$$

$$D_T = 2\mu\frac{\partial\sqrt{k_T}}{\partial X_j}\frac{\partial\sqrt{k_T}}{\partial X_j} \tag{8}$$

In addition to the transport equation for turbulent kinetic energy, an additional transport equation of laminar kinetic energy equation was introduced to describe the effect of energy transfer between mean flow fluctuations and turbulence, which is expressed as

$$\frac{D\rho k_L}{Dt} = \rho P_L + \frac{\partial}{\partial X_j}\left(\mu \frac{\partial k_T}{\partial X_j}\right) - \rho R - \rho R_{NAT} - D_L \tag{9}$$

where P_L is the production of laminar kinetic energy by large-scale turbulent fluctuations, and D_L is the near-wall dissipation of the laminar kinetic energy, which are described as:

$$P_L = \nu_{T,l} S^2 \quad ; \quad \nu_{T,l} = \underbrace{f_{\tau,l} C_{11} \left(\frac{\Omega \lambda_{eff}^2}{\nu}\right) \sqrt{k_{T,l}}\, \lambda_{eff}}_{\text{for bypass transition only}} + \underbrace{\beta_{TS} C_{12} \phi_{NAT} d^2 \Omega}_{\text{for inclusion of natural transition}}$$

$$f_{\tau,l} = 1 - e^{-C_{\tau,l}(\tau_m/\tau_{T,l})^2} \quad ; \quad \tau_{T,l} = \frac{\lambda_{eff}}{\sqrt{k_{T,l}}} \quad ; \quad k_{T,l} = k_T \left[1 - \left(\frac{\lambda_{eff}}{\lambda_T}\right)^{2/3}\right] \tag{10}$$

$$\beta_{TS} = 1 - e^{-B_{TS}^2/A_{TS}} \quad ; \quad B_{TS} = \mathrm{Max}\left\{\left(\phi_{NAT} - C_{TS,Crit}\right), 0\right\}$$

$$\Omega = \left|\nabla \times \vec{V}\right| = \sqrt{2\Omega_{ij}\Omega_{ij}} \quad ; \quad \Omega_{ij} = \frac{1}{2}\left(\frac{\partial U_i}{\partial X_j} - \frac{\partial U_j}{\partial X_i}\right)$$

$$D_L = 2\mu \frac{\partial \sqrt{k_L}}{\partial X_j} \frac{\partial \sqrt{k_L}}{\partial X_j} \tag{11}$$

In the Walters-Leylek model, the turbulent dissipation rate equation is modified as

$$\frac{D\rho\varepsilon}{Dt} = \frac{\partial}{\partial X_j}\left[\left(\mu + \frac{\alpha_T}{\sigma_k}\right)\frac{\partial \varepsilon}{\partial X_j}\right] + \rho C'_{\varepsilon 1} \frac{\varepsilon}{k_T}(P_T + R_{NAT}) - \rho C_{\varepsilon 2} \frac{\varepsilon^2}{k_T} + \rho C_{\varepsilon R} R \frac{\varepsilon^2}{\sqrt{k_T k_L}} - \frac{\varepsilon}{k_T} D_T \tag{12}$$

where $C_{\varepsilon 2}$ is a modeling constant and has a value of 1.92, and

$$C'_{\varepsilon 1} = 2\left[1 - \left(\frac{\lambda_{eff}}{\lambda_T}\right)^{\frac{4}{3}}\right] + 1.44\left(\frac{\lambda_{eff}}{\lambda_T}\right)^{\frac{4}{3}} \quad ; \quad C_{\varepsilon R} = 0.21\left(\frac{1.5\lambda_T}{\lambda_{eff}} - 1\right) \tag{13}$$

The eddy viscosity and eddy thermal diffusivity are modeled as

$$\mu_T = \mu_{T,s} + \mu_{T,l} \quad ; \quad \alpha_{\theta,T} = \frac{\mu_T}{\mathrm{Pr}_\theta} + \rho C_{\alpha,\theta} \sqrt{k_{T,l}}\, \lambda_{eff} \quad ; \quad \mathrm{Pr}_\theta = 1.5 \tag{14}$$

where $\mu_{T,s}$ and $\mu_{T,l}$ are small- and large-scale eddy viscosity, respectively. The modeling constants used in the Walters-Leylek model are listed in Table I.

Table I: Modeling Constants of the Walters-Leylek Model

C_λ	$C_{\tau,s}$	A_ν	A_0	A_s	C_μ
2.495	4360	5.5	4.04	2.12	0.09
C_R	A_{BP}	$C_{BP,Crit}$	$C_{R,NAT}$	$C_{NAT,Crit}$	A_{NAT}
0.21	8	35	4	460	120
C_{11}	C_{12}	$C_{\tau,l}$	$C_{TS,Crit}$	A_{TS}	$C_{\alpha,\theta}$
3.4×10^{-6}	6×10^{-11}	4360	1000	2000	0.035

B. Local Correlation Based Transition Model (LCTM) [40], [41]:

Since LCTM was built based on the SST model [25], the SST model is included here to illustrate the difference. The Boussinesq approximation used by the SST model can be written as

$$-\overline{\rho u_i u_j} = 2\mu_T S_{ij} - \frac{2}{3}k_T\delta_{ij} \quad ; \quad -\overline{\rho u_i h'} = \alpha_T \frac{\partial h}{\partial X_i} \tag{15}$$

where h is the mean enthalpy, u_i and h' are the fluctuation quantities of velocity components and enthalpy, and k_T, μ_T and α_T are the turbulent kinetic energy, eddy viscosity and eddy thermal diffusivity, respectively. The eddy viscosity is modeled as

$$\mu_t = \rho \frac{a_1 k_T}{\max\left(a_1\omega, |\Omega| F_2\right)}; \quad F_2 = \tanh(\arg_2^2); \quad \arg_2 = \max\left(\frac{2\sqrt{k_T}}{C_\mu \omega y}, \frac{500\nu}{y^2\omega}\right) \tag{16}$$

where ω is the specific turbulence dissipation rate, y is the normal distance away from the wall, ν is the kinematic viscosity of the fluid, a_1 (= 0.31) and C_μ (= 0.09) are the modeling constants, and

$$|\Omega| = \left|\nabla \times \vec{V}\right| = \sqrt{2\Omega_{ij}\Omega_{ij}} \quad ; \quad \Omega_{ij} = \frac{1}{2}\left(\frac{\partial U_i}{\partial X_j} - \frac{\partial U_j}{\partial X_i}\right) \tag{17}$$

The turbulent kinetic energy and specific turbulence dissipation rate are solved using the following transport equations:

$$\frac{D\rho k_T}{Dt} = P_k + \frac{\partial}{\partial X_j}\left[\left(\mu + \frac{\mu_T}{\sigma_k}\right)\frac{\partial k_T}{\partial X_j}\right] - D_k \tag{18}$$

$$\frac{D\rho\omega}{Dt} = \frac{\partial}{\partial X_j}\left[\left(\mu + \frac{\mu_T}{\sigma_\omega}\right)\frac{\partial \omega}{\partial X_j}\right] + \frac{C_k}{\nu_t}P_k - C_\omega \rho\omega^2 + 2(1-F_1)\rho\frac{1}{\sigma_{\omega 2}\omega}\frac{\partial k_T}{\partial X_j}\frac{\partial \omega}{\partial X_j} \tag{19}$$

where μ and σ_k are the fluid viscosity and modeling constant, respectively. Also,

$$D_k = \rho C_\mu k_T \omega \quad ; \quad P_k = \min\left(\mu_T S^2, 10 D_k\right) \quad ; \quad S^2 = 2S_{ij}S_{ij} \tag{20}$$

where

$$F_1 = \tanh(\arg_1^4); \quad \arg_1 = \min\left[\max\left(\frac{\sqrt{k_T}}{C_\mu \omega y}, \frac{500\nu}{y^2\omega}\right), \frac{4\rho\sigma_{\omega 2}k}{C_d y^2}\right]$$

$$C_d = \max\left(2\rho\sigma_{\omega 2}\frac{1}{\omega}\frac{\partial k_T}{\partial X_j}\frac{\partial \omega}{\partial X_j}, 10^{-20}\right); \quad \phi = F_1\phi_1 + (1-F_1)\phi_2; \quad \phi : [\sigma_k; \sigma_\omega; C_k; C_\omega] \tag{21}$$

$$\phi_1 : [\sigma_{k1} = 0.85; \quad \sigma_{\omega 1} = 2; \quad C_{k1} = 0.553; \quad C_{\omega 1} = 0.075]$$

$$\phi_2 : [\sigma_{k2} = 1; \quad \sigma_{\omega 2} = 1.168; \quad C_{k2} = 0.44; \quad C_{\omega 2} = 0.0828]$$

The eddy thermal diffusivity is modeled as

$$\alpha_T = \frac{\mu_T}{\mathrm{Pr}_T} \quad ; \quad \mathrm{Pr}_T : \text{turbulent Prandtl number} \tag{22}$$

For LCTM (a variant of the SST model), the transport equations of the turbulent kinetic energy and specific turbulent dissipation rate are modified as

$$\frac{D\rho k_T}{Dt} = \tilde{P}_k + \frac{\partial}{\partial X_j}\left[\left(\mu + \frac{\mu_T}{\sigma_k}\right)\frac{\partial k_T}{\partial X_j}\right] - \tilde{D}_k \tag{23}$$

$$\frac{D\rho\omega}{Dt} = \frac{\partial}{\partial X_j}\left[\left(\mu + \frac{\mu_T}{\sigma_\omega}\right)\frac{\partial \omega}{\partial X_j}\right] + \frac{C_k}{\nu_t}P_k - C_\omega \rho\omega^2 + 2(1-\tilde{F}_1)\rho\frac{1}{\sigma_{\omega 2}\omega}\frac{\partial k_T}{\partial X_j}\frac{\partial \omega}{\partial X_j} \tag{24}$$

where

$$\tilde{P}_k = \gamma_{\text{eff}} P_k \quad ; \quad \tilde{D}_k = \min\left[\max\left(\gamma_{\text{eff}}, 0.1\right), 1.0\right] D_k$$

$$\gamma_{\text{eff}} = \max\left(\gamma, \gamma_{\text{sep}}\right) \quad ; \quad \gamma_{\text{sep}} = \min\left\{8\max\left[\left(\frac{\text{Re}_{\text{v}}}{2.193\text{Re}_{\theta c}}\right) - 1, 0\right] F_{\text{reattach}}, 5\right\} F_{\theta t}$$

$$F_{\text{reattach}} = e^{-(R_T/15)^4} \quad ; \quad R_T = \frac{\rho k_{\text{T}}}{\mu\omega} \quad ; \quad \text{Re}_{\text{v}} = \frac{\rho y^2 S}{\mu} \quad ; \quad \text{Re}_{\theta c} = \frac{\rho U_\infty \theta_c}{\mu} \tag{25}$$

$$F_{\theta t} = \min\left\{\max\left[F_{\text{wake}} e^{-(y/\delta)^4}, 1 - \left(\frac{C_{e2}\gamma - 1}{C_{e2} - 1}\right)^2\right], 1\right\} \quad ; \quad F_{\text{wake}} = e^{-(\text{Re}_\omega \times 10^{-5})^2}$$

$$\text{Re}_\omega = \frac{\rho\omega y^2}{\mu} \quad ; \quad \delta = \frac{50\Omega y}{U}\delta_{\text{BL}} \quad ; \quad \delta_{\text{BL}} = 7.5\theta_{\text{BL}} \quad ; \quad \theta_{\text{BL}} = \frac{\overline{\text{Re}_{\theta t}}\,\mu}{\rho U}$$

$$\tilde{F}_1 = \max\left(F_1, F_3\right) \quad ; \quad F_3 = e^{-(R_y/120)^8} \quad ; \quad R_y = \frac{\rho y\sqrt{k_{\text{T}}}}{\mu}$$

where θ_c is the critical momentum thickness. LCTM solves two extra transport equations to account for the transition effect. The first one is the intermittency (γ) equation used to trigger the transition process. The second one is formulated in terms of the local transition momentum thickness Reynolds number ($\overline{\text{Re}_{\theta t}}$) to avoid additional non-local operations introduced by the quantities used in empirical correlations.

1) Intermittency Equation:

$$\frac{D\rho\gamma}{Dt} = \frac{\partial}{\partial X_j}\left[\left(\mu + \frac{\alpha_{\text{T}}}{\sigma_\gamma}\right)\frac{\partial\gamma}{\partial X_j}\right] + P_{\gamma 1} - E_{\gamma 1} + P_{\gamma 2} - E_{\gamma 2} \tag{26}$$

where transition source terms are defined as:

$$P_{\gamma 1} = F_{\text{length}} C_{a1}\rho S[\gamma F_{\text{onset}}]^{C_\alpha} \quad ; \quad E_{\gamma 1} = C_{e1} P_{\gamma 1}\gamma \quad ; \quad P_{\gamma 2} = C_{a2}\rho\Omega\gamma F_{\text{turb}} \quad ; \quad E_{\gamma 2} = C_{e2} P_{\gamma 2}\gamma$$

$$F_{\text{turb}} = e^{-(R_T/4)^4} \quad ; \quad F_{\text{onset}} = \max\left[\left(F_{\text{onset},2} - F_{\text{onset},3}\right), 0\right]$$

$$F_{\text{onset},2} = \min\left[\max\left(F_{\text{onset},1}, F_{\text{onset},1}^4\right), 2\right] \quad ; \quad F_{\text{onset},1} = \frac{\text{Re}_{\text{v}}}{2.193\text{Re}_{\theta c}} \tag{27}$$

$$F_{\text{onset},3} = \max\left[1 - \left(\frac{R_T}{2.5}\right)^3, 0\right] \quad ; \quad \text{Re}_{\theta c} = f\left(\overline{\text{Re}_{\theta t}}\right) \quad ; \quad F_{\text{length}} = g\left(\overline{\text{Re}_{\theta t}}\right)$$

The correlations for calculating three empirical parameters, F_{length}, $\text{Re}_{\theta c}$, and $\text{Re}_{\theta t}$ were not provided in Menter's original paper [40], [41]. F_{length} is used to control the length of the transition zone and $\text{Re}_{\theta c}$ (the critical momentum thickness Reynolds number) is used to control the onset of the transition location. Suluksna and Juntasaro [45] suggested that for bypass transition $\text{Re}_{\theta c}$ can be set to $\text{Re}_{\theta t}$ (transition onset momentum thickness Reynolds number), and F_{length} and $\text{Re}_{\theta c}$ can be obtained from the following correlation.

$$\text{Re}_{\theta c} = \text{Re}_{\theta t} = 803.73\left(Tu_{\infty,\text{le}} + 0.6067\right)^{-1.027} F\left(\lambda_\theta, K\right) \quad ; \quad F_{\text{length}} = 163\ln\left(Tu_{\infty,\text{le}}\right) + 3.625 \tag{28}$$

where $Tu_{\infty,\text{le}}$ is the freestream turbulence intensity at the leading edge, and $F(\lambda_\theta, K)$ is an empirical parameter used to account for the pressure gradient effect which can be calculated as

$$F(\lambda_\theta, K)=\begin{cases} 1-F_\lambda e^{-Tu/3}; & \lambda_\theta \le 0 \\ 1+F_K\left(1-e^{-Tu/1.5}\right)+0.556\left(1-e^{-23.9\lambda_\theta}\right); & \lambda_\theta > 0 \end{cases}$$

$$\lambda_\theta=\frac{\rho\theta^2}{\mu}\frac{dU}{ds} \quad ; \quad \frac{dU}{ds}=\frac{\mathrm{u}}{U}\frac{dU}{dx}+\frac{\mathrm{v}}{U}\frac{dU}{dy}+\frac{\mathrm{w}}{U}\frac{dU}{dz} \quad ; \quad U=\sqrt{\mathrm{u}^2+\mathrm{v}^2+\mathrm{w}^2}$$

$$K=\frac{\mu}{\rho U^2}\frac{dU}{ds} \quad ; \quad F_\lambda=-10.32\lambda_\theta-89.47\lambda_\theta^2-265.51\lambda_\theta^3 \qquad (29)$$

$$F_K=0.0962\left(K\times10^6\right)+0.148\left(K\times10^6\right)^2+0.0141\left(K\times10^6\right)^3$$

$$-3\times10^{-6}\le K\le 3\times10^{-6} \quad ; \quad -0.1\le\lambda_\theta\le 0.1 \quad ; \quad \mathrm{Re}_{\theta t}\ge 20$$

We will denote the above empirical correlation as the S-J correlation. In the course of this study, it was found that the S-J correlation is only valid for $0.98 < Tu_{\infty,\mathrm{le}} < 7$, and the assumption of $\mathrm{Re}_{\theta c} = \mathrm{Re}_{\theta t}$ is limited to bypass transition and thus does not work well in simulating the hypersonic transition flow. Though empirical correlations for calculating F_{length} and $\mathrm{Re}_{\theta c}$ based on $\overline{\mathrm{Re}_{q t}}$ were not available in [40]-[41], an empirical correlation of $\mathrm{Re}_{\theta t}$ (different from that suggested by Suluksna and Juntasaro [45]) was found in Langtry's dissertation [46]. This correlation is expressed as

$$\mathrm{Re}_{\theta t}=\begin{cases} \left[1173.51-589.428Tu+\dfrac{0.2196}{Tu^2}\right]F(\lambda_\theta); & \text{if } Tu\le 1.3 \\ 331.5[Tu-0.5658]^{-0.671}F(\lambda_\theta); & \text{if } Tu>1.3 \end{cases}$$

$$F(\lambda_\theta)=\begin{cases} 1-\left(-12.986\lambda_\theta-123.66\lambda_\theta^2-405.689\lambda_\theta^3\right)e^{-(Tu/1.5)^{1.5}}; & \lambda_\theta\le 0 \\ 1+0.275\left[1-e^{-35\lambda_\theta}\right]e^{-(Tu/0.5)}; & \lambda_\theta>0 \end{cases} \qquad (30)$$

$$Tu=100\frac{\sqrt{2k_{\mathrm{T}}/3}}{U}$$

$$-0.1\le\lambda_\theta\le 0.1 \quad ; \quad Tu\ge 0.027 \quad ; \quad \mathrm{Re}_{\theta t}\ge 20$$

In this study, Nichols (a member of this research team) developed a new set of empirical correlations for F_{length} and $\mathrm{Re}_{\theta c}$ based on the above correlation and test cases employed here, and adding the pressure gradient effect into the above correlation. This set of empirical correlation is denoted as the N-L correlation, and is listed in the following:

$$\mathrm{Re}_{\theta c}=\mathrm{Re}_{\theta t}\left(-4.45\times10^4\,\mathrm{Re}_{\theta t}+0.92\right) \quad ; \quad F_{\mathrm{length}}=8.5\times10^7\,\mathrm{Re}_{\theta t}^{-3}\left(1+0.25M^4\right)$$

$$\mathrm{Re}_{\theta t}=\begin{cases} \left[1173.51-589.428Tu+\dfrac{0.2196}{Tu^2}\right]F(\lambda_\theta); & \text{if } Tu\le 1.3 \\ 331.5[Tu-0.5658]^{-0.671}F(\lambda_\theta); & \text{if } Tu>1.3 \end{cases}$$

$$F(\lambda_\theta)=\begin{cases} 1-\left(-12.986\lambda_\theta-123.66\lambda_\theta^2-405.689\lambda_\theta^3\right)e^{-(Tu/1.5)^{1.5}}; & \lambda_\theta\le 0 \\ 1+0.275\left[1-e^{-35\lambda_\theta}\right]e^{-(Tu/0.5)}; & \lambda_\theta>0 \end{cases} \qquad (31)$$

$$\lambda_\theta=\frac{\rho\theta^2}{\mu}\frac{dU}{ds}F_c \quad ; \quad F_c=\left[1+16(2M)^4\right]^{\frac{1}{4}}$$

$$-0.1\le\lambda_\theta\le 0.1 \quad ; \quad Tu\ge 0.027 \quad ; \quad \mathrm{Re}_{\theta t}\ge 20$$

where F_c is the correction factor for the pressure gradient effect in high-speed flows, and M is the local flow Mach number. It should be noted that both S-J and N-L correlations provide F_{length} and $\text{Re}_{\theta c}$ as functions of $\text{Re}_{\theta t}$ instead of $\overline{\text{Re}_{\theta t}}$, which was proposed in the original LCTM.

2) Local Transition Onset Momentum Thickness Reynolds Number Equation:

$$\frac{D\rho\overline{\text{Re}_{\theta t}}}{Dt} = P_{\theta t} + \frac{\partial}{\partial X_j}\left[\sigma_{\theta t}(\mu+\mu_T)\frac{\partial\overline{\text{Re}_{\theta t}}}{\partial X_j}\right] \tag{32}$$

where the source term is defined as

$$P_{\theta t} = \frac{C_{\theta t}}{\tau_{\theta t}}\rho\left(\text{Re}_{\theta t} - \overline{\text{Re}_{\theta t}}\right)\left(1-F_{\theta t}\right) \quad ; \quad \tau_{\theta t} = \frac{500\mu}{\rho U^2} \quad ; \quad \text{Re}_{\theta t} = \frac{\rho U_\infty \theta_t}{\mu} \tag{33}$$

The modeling constants used in LCTM are listed in Table II.

Table II: Modeling Constants of LCTM

C_{a1}	C_{a2}	C_{α}	C_{e1}	C_{e2}	σ_{γ}	$C_{\theta t}$	$\sigma_{\theta t}$	C_{e2}
2	0.06	0.5	1	50	1	0.03	2	50

The LCTM with both S-J and N-L correlations has been implemented into the OVERFLOW-2.1 code [47], [48], while both the Walters-Leylek model and LCTM (S-J correlation only) have been implemented into the FDNS code [49]-[51] for assessment under this project. The results of our assessment from this study are detailed herein.

IV. ASSESSMENT RESULTS

Under this project, three groups of benchmark turbulence transition test cases were employed to assess the validity and performance of the Walters-Leylek model and LCTM. These three groups of experimental tests are: (1) subsonic flow over a flat plate [52], (2) hypersonic flow over a cylindrical cone [7], [8], and (3) subsonic flow over a turbine stator cascade [53], [54]. The results and assessment for these test cases are reported herein.

A. Subsonic Flow over a Flat Plate

A series of experimental studies of a subsonic flow over a flat plate (also known as T3 series) conducted by Coupland [52] were selected to evaluate the Walters-Leylek model and LCTM. Three test cases of the T3 series were examined in this study, and their freestream conditions are listed in Table III. The computational mesh system (265×100 points) is plotted in Fig. 1. Two sets of results for each test case are presented here; one set is obtained by using the FDNS code, and the other is from the OVERFLOW code. The study done by using the FDNS code is concentrated on comparing different turbulence transition models and the effect of near-wall grid spacing; whereas the result from the OVERFLOW code is used to demonstrate the impact of different empirical correlations (S-J [45] vs. N-L) on LCTM. It should be noted that the numerical results obtained with LCTM in this study may differ from those obtained with the original LCTM because its empirical correlations are not completely available to us.

Table III: Freestream Conditions and Downstream Boundary Conditions for T3 Series of Test Cases

Case	Upstream velocity (m/s)	Upstream turbulence intensity (%)	Pressure gradient
T3A	5.4	3.5	Zero
T3B	9.4	6.0	Zero
T3AM	19.8	0.9	Zero

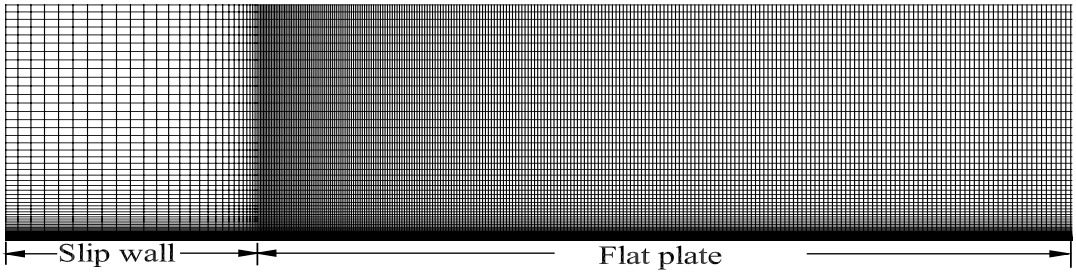

Fig. 1: Computational grid used for simulations of T3 test cases

1) T3A Test Case:

The results from the FDNS code are presented first to show the comparison among different turbulence transition models and the effect of near-wall grid spacing. The skin friction coefficient distributions along the flat plate predicted by different turbulence models are compared in Fig. 2. Since the Walters-Leylek model is constructed based on the Low-Re k-ε model and LCTM is a modification of the Shear Stress Transport (SST) model, the results obtained from the baseline Low-Re k-ε model and the baseline SST model are also included to demonstrate the difference due to the transition effect. It can be seen that both the Walters-Leylek model and LCTM properly capture the transition effect and the onset of transition, but predict a smaller transition zone than the test data. Different near-wall grid spacings were also employed for both transition models to demonstrate the effect of grid dependence. The results are illustrated using the plot of the non-dimensionalized streamwise velocity (u^+) vs. the non-dimensionalized distance away from the wall (y^+), and are shown in Fig. 3. The u^+ profile is taken at the streamwise location in the middle of the transition zone (595 mm from the leading edge of the flat plate). It can be seen that LCTM is more sensitive to the near-wall grid resolution than the Walters-Leylek model. Though neither model predicts the velocity profile matching the test data, the result is considered to be reasonably good.

The large difference in the near-wall velocity profiles predicted by LCTM with different near-wall grid resolutions is attributed to the variation of predicted transition locations, which can be seen in Fig. 4. In Fig. 5, freestream turbulence intensity distributions along the axial direction predicted by both transition models are compared to the test data. It is shown that both models are unable to accurately predict the decay of the freestream turbulence intensity. However, this comparison should be viewed as a qualitative trend only for the following reasons. The first reason is that though the upstream turbulence intensity level is provided, the location corresponding to the given turbulence level is not available in the literature, and this has an impact on the freestream turbulence level at downstream. Hence, it was numerically estimated in this study.

The second reason is that there is uncertainty in the correlation between the turbulence intensity and the calculated turbulent kinetic energy because of the assumption of isotropic turbulence in the employed turbulence models. The third reason is that the location where the freestream turbulence intensity was measured is not defined, and thus in the present study the values of the turbulent kinetic energy at the far field boundary (700 mm from the wall) were used for comparison. Nevertheless, the decay of turbulence intensity predicted by LCTM is slightly better than that by the Walters-Leylek model.

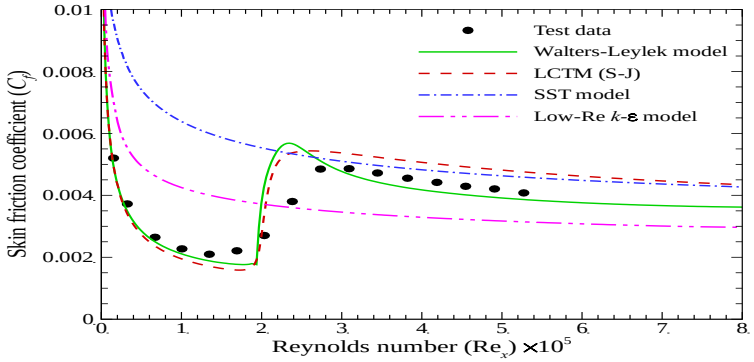

Fig. 2: Comparisons of skin friction coefficient distribution for T3A test case

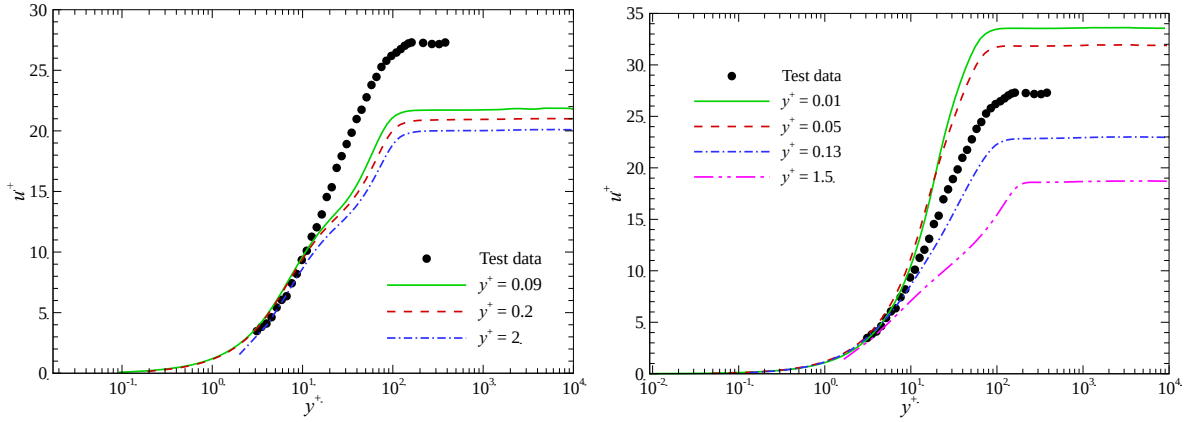

(a) Walters-Leylek model (b) LCTM (S-J)

Fig. 3: Comparisons of non-dimensionalized near-wall velocity profile for T3A test case

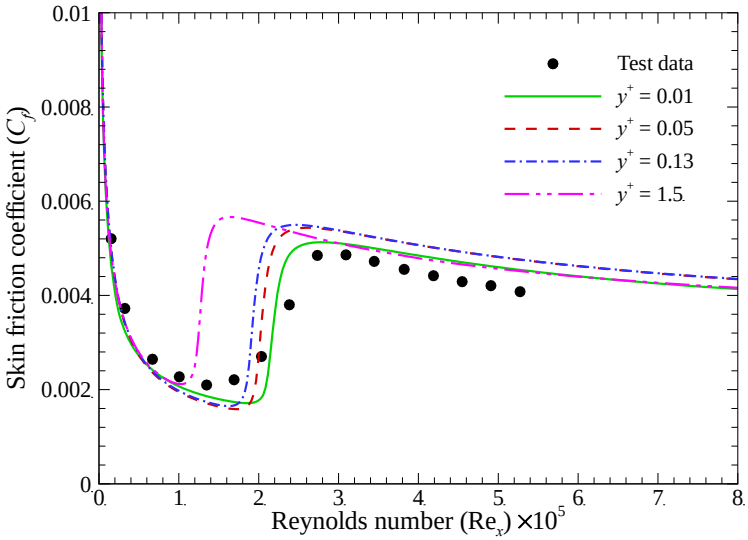

Fig. 4: Skin friction coefficient distribution predicted by LCTM (S-J) with different near-wall grid resolutions

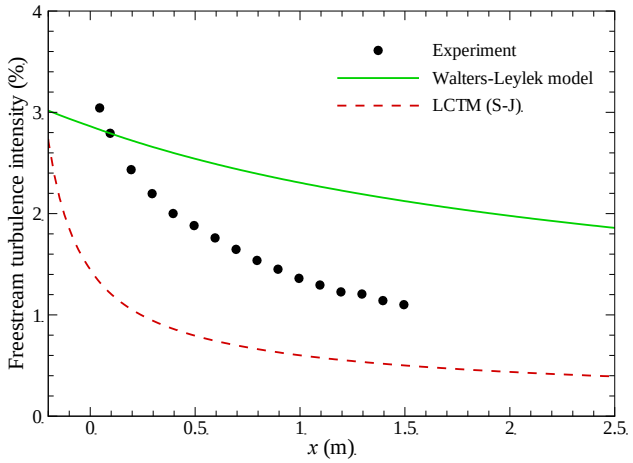

Fig. 5: Comparisons of freestream turbulence intensity distribution for T3A test case

The results obtained from the OVERFLOW code using LCTM with both S-J and N-L correlations are compared in Fig. 6. It can be seen that the N-L correlation performs better than the S-J correlation in predicting the location of transition onset.

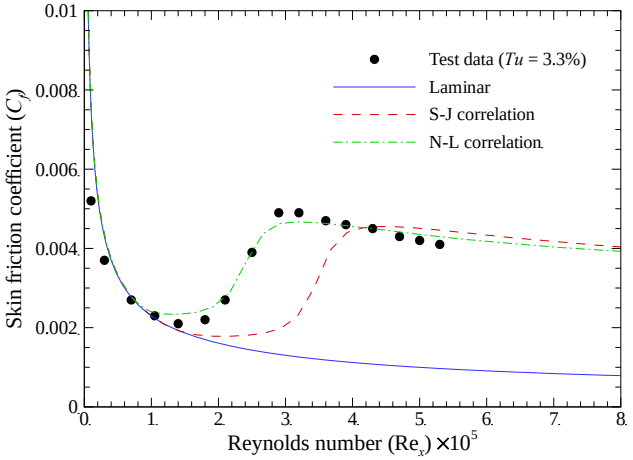

Fig. 6: Comparisons of skin friction coefficient distribution predicted by LCTM with different empirical correlations

2) T3B Test Case:

As shown in Table 3, the T3B test case has higher upstream velocity and turbulence intensity than the T3A test case. Hence, it is expected that turbulence transition should occur earlier. This is confirmed by the plot of skin friction coefficient distribution along the flat plate as shown in Fig. 7. It can be seen that the Walters-Leylek model and LCTM properly capture both the onset of transition and the transition zone. Comparing to the T3A test case, both transition models perform better in predicting the transition effect in the T3B case, which has higher upstream turbulence intensities. This is consistent with the fact that both models were developed based on the assumption of bypass transition, which occurs at high turbulence intensities. Grid sensitivity studies were also conducted for this test case, and the result is demonstrated using the near-wall velocity (u^+) profile as shown in Fig. 8. For this test case, the u^+ profile is plotted at 145 mm downstream from the leading edge of the flat plate, which is in the middle of the transition zone. Once again, LCTM is shown to be more sensitive to the near-wall grid resolution than the Walters-Leylek model. Hence, the transition location predicted by LCTM, shown in Fig. 7, is expected to vary with different near-wall grid spacings. This becomes a major concern about LCTM in addition to others mentioned earlier. Similar to the skin friction coefficient distribution, the predicted velocity profiles of the T3B test case have better agreement with the test data when compared to those of the T3A test case due to higher upstream turbulence intensity. This phenomenon can also be observed in the freestream turbulence intensity distribution, shown in Fig. 9. It can be seen that the decay of freestream turbulence intensity predicted by those two transition models agree better with the test data both qualitatively and quantitatively. Once again, this comparison should be viewed as a reference measure and should not be emphasized too much due to the aforementioned reasons. Overall, both models perform well in capturing the transition effect of the T3B test case. Fig. 10 demonstrates the comparison of the results between the S-J and N-L correlations of LCTM obtained from the OVERFLOW-2.1 code. Once again, the N-L correlation captures the transition zone better than the S-J correlation.

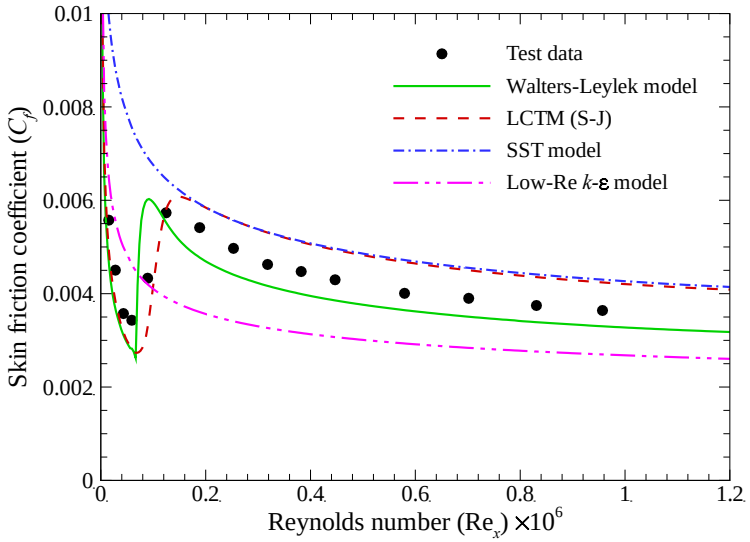

Fig. 7: Comparisons of skin friction coefficient distribution for T3B test case

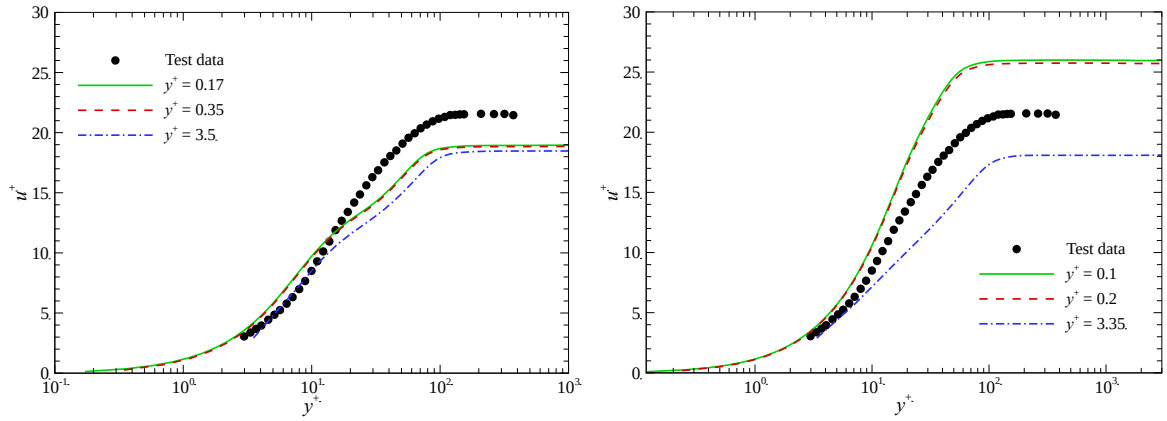

(a) Walters-Leylek model (b) LCTM (S-J)

Fig. 8: Comparisons of non-dimensionalized near-wall velocity profile for T3B test case

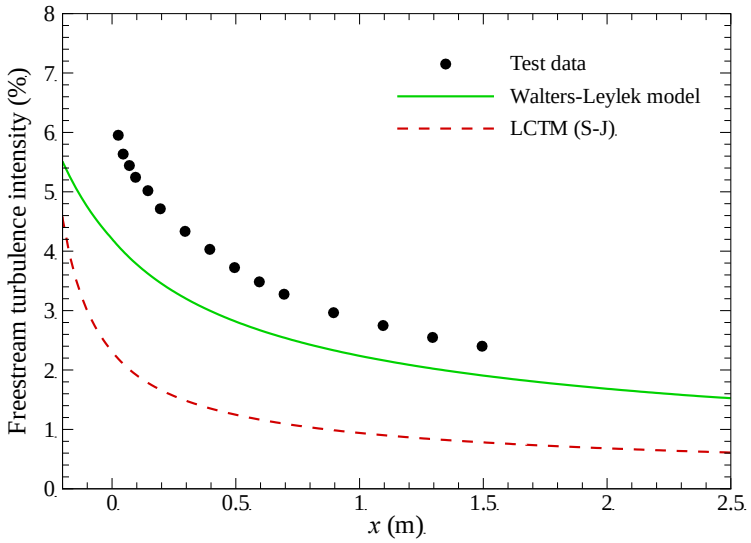

Fig. 9: Comparisons of freestream turbulence intensity distribution for T3B test case

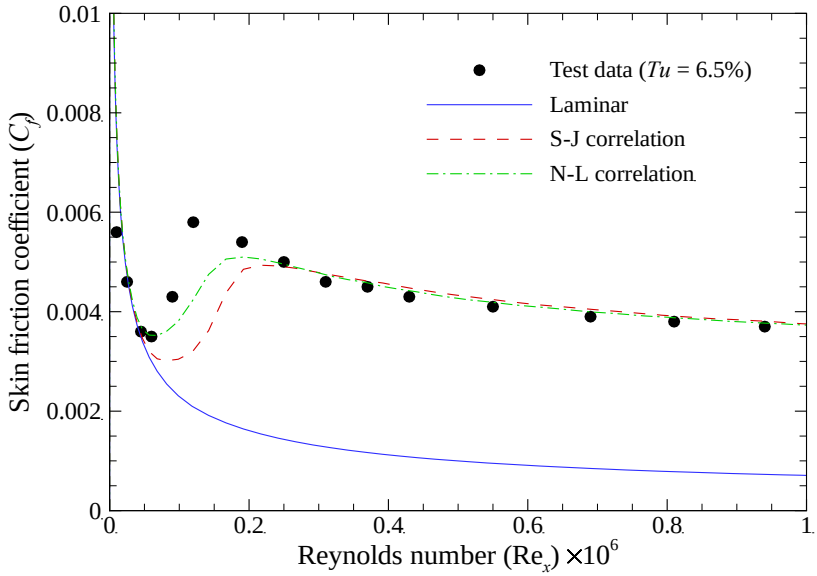

Fig. 10: Comparisons of skin friction coefficient distribution predicted by LCTM with different empirical correlations

3) T3AM Test Case:

The T3AM test case has the highest upstream velocity and the lowest turbulence intensity among all three flat plate test cases. With this test case, which has different trends in varying upstream velocity and turbulence intensity magnitudes, we can evaluate which has a stronger effect on turbulence transition, the upstream velocity or turbulence magnitude. The skin friction coefficient distribution, shown in Fig. 11, indicates that not only transition occurs later (i.e. further downstream) but also the transition zone is larger. This indicates that the upstream turbulence intensity is the main driver for both transition to turbulent flow regime and switching from natural transition to bypass transition as the upstream turbulence intensity increases. Since the T3AM test case has the lowest freestream turbulence intensity, the effect of natural transition becomes more important. Both transition models evaluated here were developed based on the bypass transition assumption, and are expected to not perform as well for this case. This is confirmed by the result shown in Fig. 11. It can be seen that both the Walters-Leylek model and LCTM fail to capture the onset of transition. The result of a grid sensitivity study for this test case is demonstrated in the near-wall velocity profile comparison shown in Fig. 12. For this test case, the u^+ profile is plotted at 1095 mm downstream from the leading edge of the flat plate, which is in the middle of the transition zone. Once again, LCTM is shown to be more sensitive to the near-wall grid resolution than the Walters-Leylek model. Moreover, the discrepancy between the numerical results of both models and the test data is larger for this test case than that for the other two test cases. This error is caused by

failure of capturing the transition location. The deficiency of these two transition models in resolving the transition effect with the low upstream turbulence level can also be observed in the freestream turbulence intensity distribution shown in Fig. 13. It can be seen that both models fail to predict both the decay and magnitude of freestream turbulence intensity. In Fig. 14, the result of the N-L correlation is compared with that of the S-J correlation for the OVERFLOW implementation. It can be seen that the N-L correlation predicts slightly early transition, while the S-J correlation fails to capture the transition effect. Once again, the comparison of LCTM should be viewed as a qualitative assessment and should not be used to measure the performance of the transition models due to the uncertainty of the empirical correlations employed. Overall, both models have the worst performance in capturing the transition effect for the T3AM test case due to its low upstream turbulence intensity.

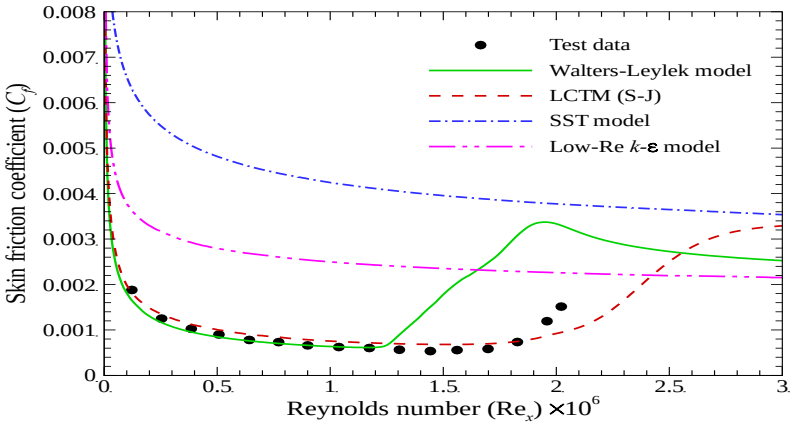

Fig. 11: Comparisons of skin friction coefficient distribution for T3AM test case

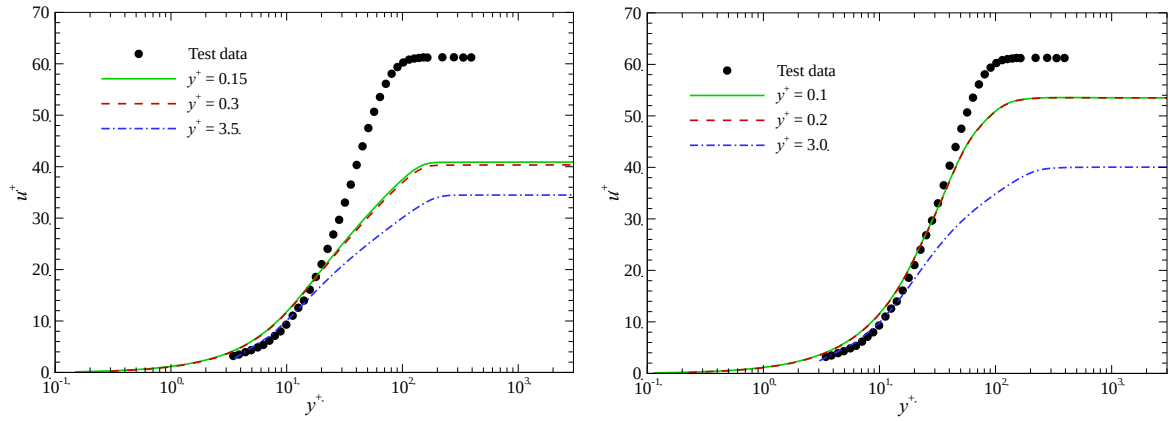

(a) Walters-Leylek model (b) LCTM (S-J)

Fig. 12: Comparisons of non-dimensionalized near-wall velocity profile for T3AM test case

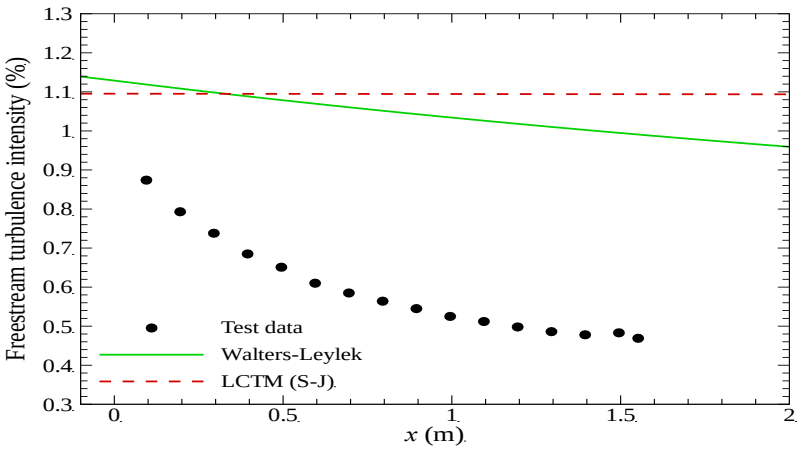

Fig. 13: Comparisons of freestream turbulence intensity distribution for T3AM test case

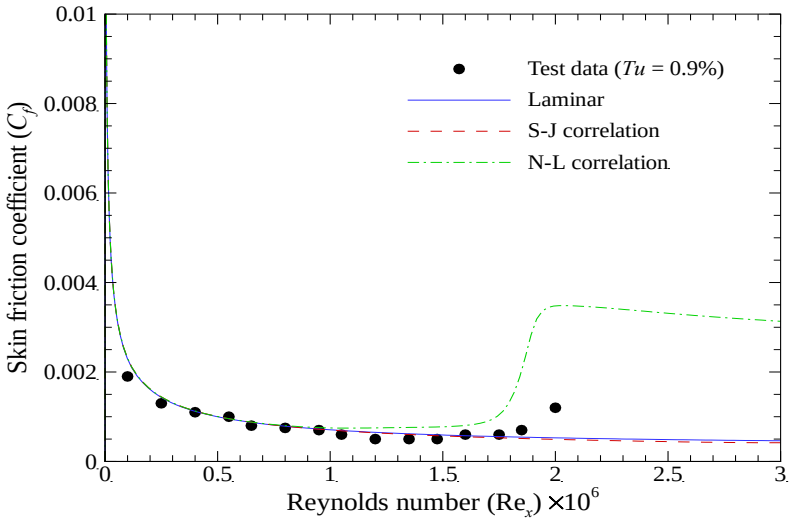

Fig. 14: Comparisons of skin friction coefficient distribution predicted by LCTM with different empirical correlations

B. Hypersonic Flow over a Cylindrical Cone

A hypersonic flow over a set of 7° sharp cone cylinders (Kimmel [7], [8]) was used to evaluate the Walters-Leylek model and LCTM in this study. The surface geometry of the set of cylindrical cones to account for the effect of different pressure gradients is illustrated in Fig. 15a, while the computational mesh system for the case of dp/dx = 1 (109×75 points) is plotted in Fig. 15b. The free stream and wall boundary conditions of this set of test cases are listed in Table IV.

Table IV: Freestream Conditions and Wall Boundary Conditions for Kimmel's Test Case

Upstream Mach no.	Reynolds number	Upstream total temperature	Wall temperature
7.93	6.6×10^6 m^{-1}	722 K	303.24 K

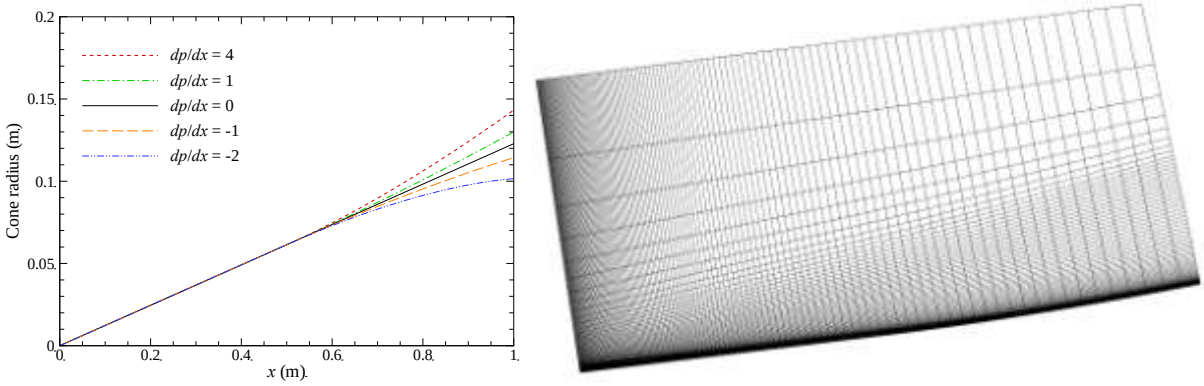

(a) (b)

Fig. 15: Cone geometry and computational grid for simulations of Kimmel's hypersonic flow test case

Different turbulence models were tested using the FDNS code. Grid sensitivity studies of the turbulence transition models were performed using four different near-wall grid resolutions (Grid #1: y^+ = 2.5, Grid #2: y^+ = 0.4, Grid #3: y^+ = 0.2, and Grid #4: y^+ = 0.1) in evaluating the turbulence models. Since the freestream turbulence intensity was not reported in [7] and [8], a freestream turbulence intensity of 0.5% is selected in evaluating the turbulence transition model with different near-wall grid resolutions. In this study, a dimensionless heat transfer coefficient near the wall (Stanton number, St) was used to assess the accuracy of the turbulence transition models. The Stanton number is defined as

$$St = \frac{q_w}{\rho_\infty u_\infty (h_{0\infty} - h_w)} \qquad (34)$$

where q_w is the heat flux to the wall, and ρ_∞ and u_∞ are the freestream density and velocity, respectively, h_w is the enthalpy at the wall, and $h_{0\infty}$ is the freestream stagnation enthalpy upstream of the shock.

The Stanton number distributions along the cone surface with zero pressure gradient (dp/dx = 0) are predicted by different turbulence models using four different near-wall grid resolutions. The numerical results are compared to the test data, and plotted as shown in Fig. 16. From this figure, we can observe that (1) the performance of all turbulence models is very sensitive to the near-wall grid resolution, (2) near-wall grid spacing ($y^+ < 0.1$) is very critical to capturing the transition effect in the hypersonic flow due to very thin boundary layer, (3) the Walters-Leylek model does capture the transition effect but predicts early transition onset, and (4) LCTM with the S-J correlation fails to capture the transition effect.

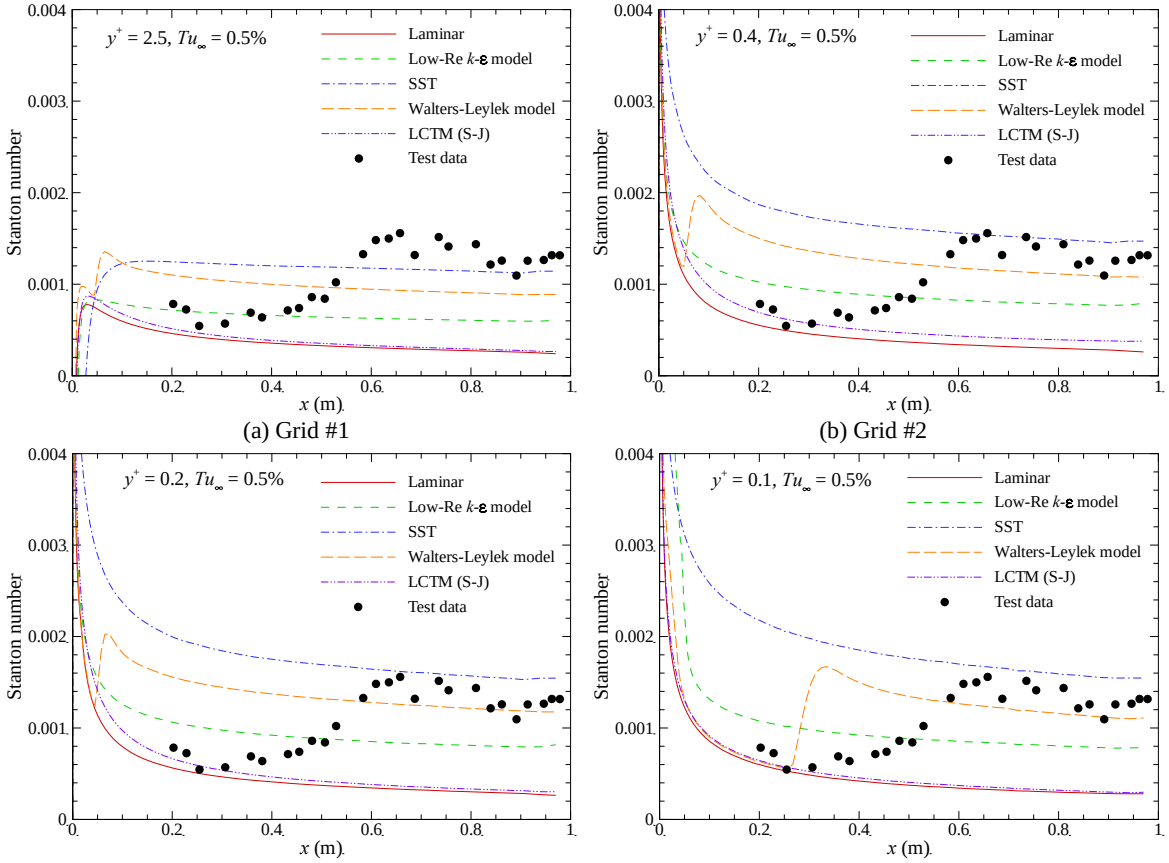

(a) Grid #1 (b) Grid #2

(c) Grid #3 (d) Grid #4

Fig. 16: Comparison of Stanton number distribution along cone surface for different near-wall grid resolutions (dp/dx = 0)

In the study of T3 series subsonic flat plate test cases, the LCTM with the N-L correlation was shown to have better prediction of turbulence transition than the S-J correlation. Hence, the LCTM with the N-L correlation implemented in the OVERFLOW code was also employed to compute this hypersonic cylindrical cone case with zero pressure gradient. Furthermore, since the freestream turbulence intensity was not reported in [7] and [8], a sensitivity study was also conducted. The near-wall grid resolution for this study is y^+ = 0.1. Four different turbulence intensity levels in the freestream (Tu_∞ = 0.25%, 0.5%, 1%, and 2%) were tested, and the results are shown in Fig. 17, which reveals that the transition location for hypersonic flows is sensitive to the freestream intensity prescribed. The transition results are bounded by the fully turbulent (SST model) and laminar solutions from OVERFLOW. In addition, the N-L correlation is shown to perform better than the S-J correlation in capturing turbulence transition for the same freestream turbulence intensity. Further study of other hypersonic flow test cases, which provide freestream turbulence intensity, is needed to give a fair assessment of the turbulence transition model.

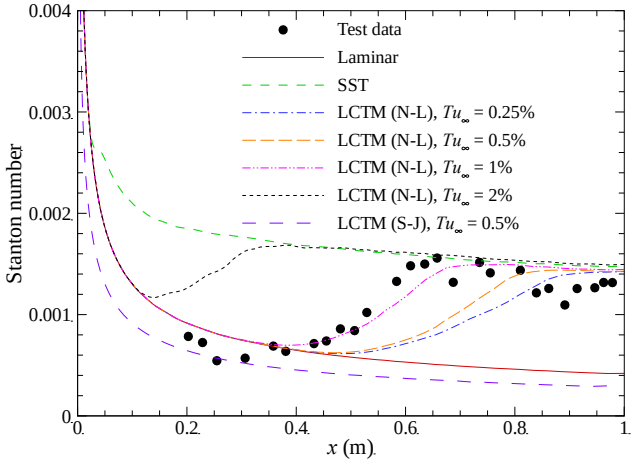

Fig. 17: Comparisons of Stanton number distribution along cone surface predicted by LCTM with different freestream turbulence intensity and two empirical correlations

To examine the effect of pressure gradient on the transition models, the hypersonic flow over a flared cone (dp/dx = -1, -2, 1, and 4) by Kimmel [7]-[8] was computed and compared. In this series of computations, the freestream turbulence intensity was set to be 0.5%. Calculations with different near-wall grid resolutions (y^+ = 0.4, y^+ = 0.2, and y^+ = 0.1) were performed for each cone geometries, and the trend of heat transfer to grid sensitivity is similar to that of the zero-pressure gradient case. Hence, only the results of y^+ = 0.1 are reported here, as shown in Fig. 18, to illustrate the comparisons. It can be seen that the Walters-Leylek model can qualitatively capture the transition and pressure gradient effects, but predicts early transition onset and small transition zone as for the zero pressure gradient case. The LCTM with the S-J correlation once again fails to capture the transition characteristics for various pressure gradient effects.

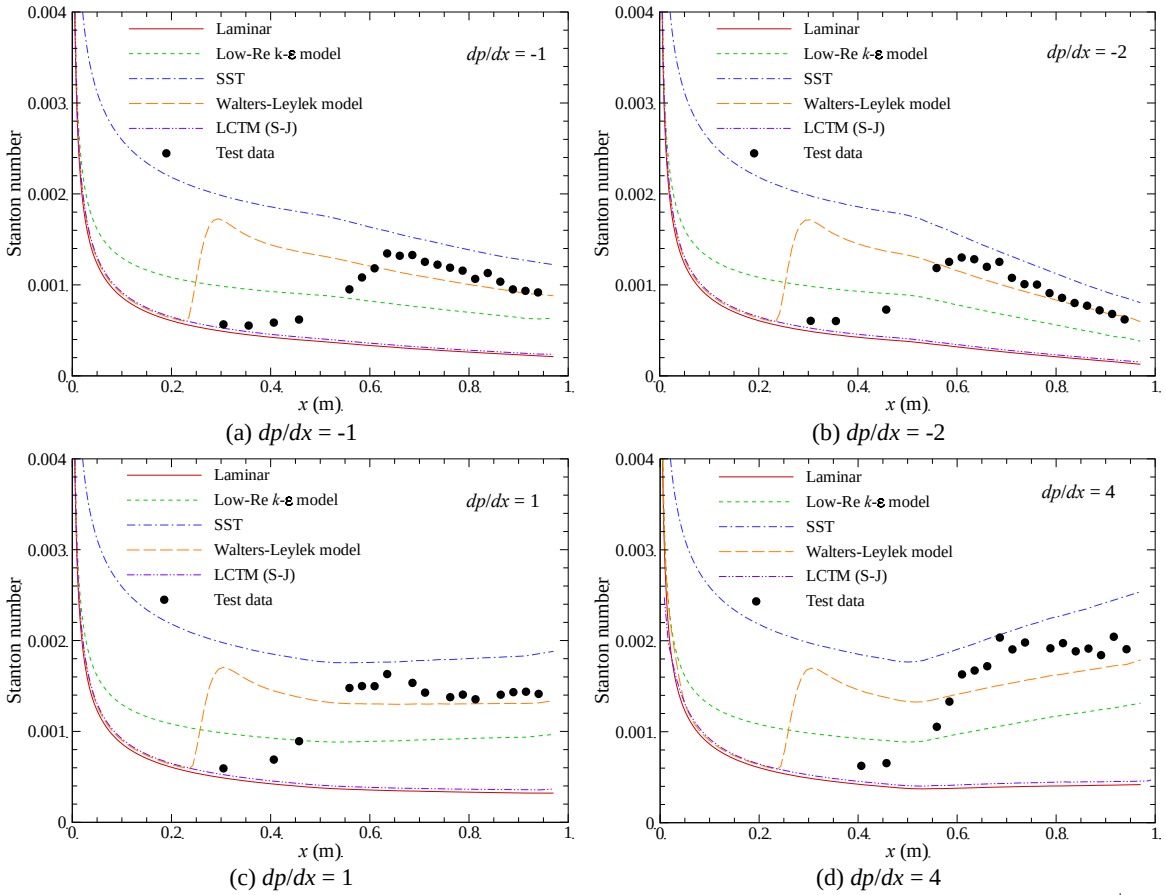

(a) dp/dx = -1 (b) dp/dx = -2

(c) dp/dx = 1 (d) dp/dx = 4

Fig. 18: Comparison of Stanton number distribution along cone surface for different pressure gradients (y^+ = 0.1, Tu_∞ = 0.5%)

C. Subsonic Flow over a Turbine Stator Cascade

The third set of selected test cases is a subsonic flow around a turbine stator cascade, tested by Radomsky and Thole [53]-[54]. Unlike the previous two sets of test cases, boundary layers developing on the blade surface of this case are subjected to the effect of surface curvature in addition to turbulence transition, freestream turbulence levels, pressure gradients, etc. Hence, this case is more complicated than the flat-plate test case. The free stream conditions of this test case are set to be uniform with zero cross-flow velocity, and are listed in Table V. The Reynolds number is based on the chord length of the stator blade (0.59 m). Three different freestream turbulence levels were tested in [53]-[54], but only the case with highest turbulence intensity (Tu_∞ = 19.5%) simulating the exhaust gas from a combustor is examined to study its effect on pressure loads and heat transfer. Based on the test data, the freestream dissipation length scale was set to be 27% of the blade pitch, which is 77% of the blade chord length. The wall temperature around the stator blade was not reported in the open literature, and thus is set to be 300 K in the present evaluation study. A periodic boundary condition in the pitching direction is employed. This allows the use of one blade passage to represent the entire cascade. Flow variation in the spanwise direction is assumed to be negligible so that 2-D numerical simulations may be performed. A combination of H-type and O-type grids is employed to generate a structured multi-block mesh system as shown in Fig. 19. The mesh system consists of 5 blocks, which have 74×90, 364×25, 150×25, 150×30, and 79×83 grid points, respectively.

Table V: Freestream Conditions for Subsonic Flow over a Turbine Stator Cascade

Pressure	Temperature	Velocity	Reynolds number
1 atm	293 K	5.85 m/s	2.3×10^5

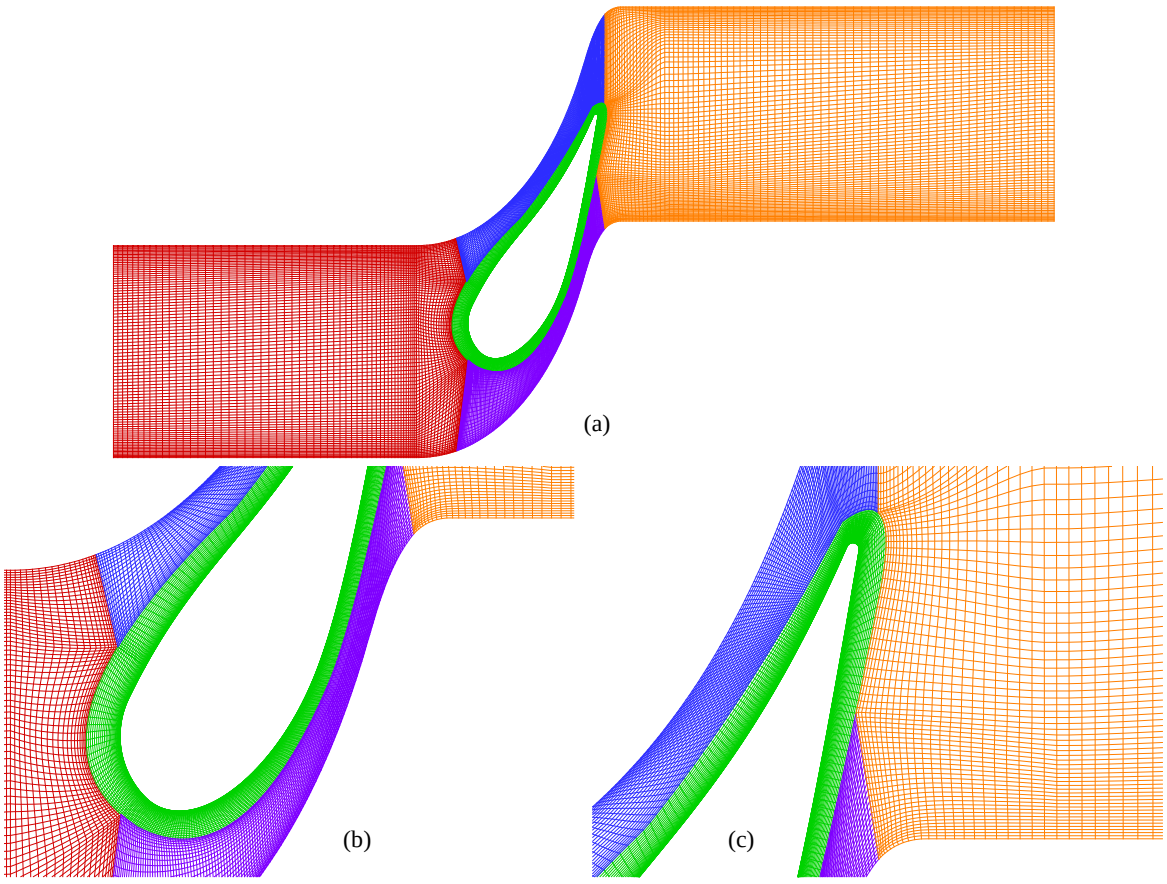

Fig. 19: Computational mesh for a subsonic flow over a turbine stator cascade; (a) entire domain, (b) near the leading edge, (c) near the trailing edge

For this test case, the test data of both the pressure coefficient (C_p) and Stanton number (St) are used to assess the accuracy of the turbulence transition models, and they are defined as

$$C_p = \frac{p - p_\infty}{\frac{1}{2}\rho_\infty u_\infty^2} \quad ; \quad St = \frac{q_w}{\rho_\infty u_\infty (h_{0\infty} - h_w)} \tag{35}$$

where q_w is the heat flux to the blade surface, p and h_w are the pressure and enthalpy at the blade surface, and ρ_∞, p_∞, $h_{0\infty}$ and u_∞ are the freestream density, pressure, stagnation enthalpy and velocity, respectively. To investigate the effect of grid dependence three near-wall grid resolutions (y^+ = 0.2, 0.1, and 0.05) were employed to simulate this test case. The Walters-Leylek model [38], the LCTM [40]-[41] with S-J correlations [45], the low-Re k-ε model [24], and the SST model [25], implemented in the FDNS code, are evaluated with these three near-wall grid resolutions. The LCTM with N-L correlations, implemented in the OVERFLOW code, is assessed with the near-wall resolution of y^+ = 0.1 only.

The pressure coefficient and Stanton number distributions along the blade surface predicted by different turbulence models with different near-wall grid resolution are compared to the test data, and are plotted as shown in Figs. 20-22, respectively. In the x-axis, S is the surface distance along the blade measured from its stagnation point, where the distance on the pressure side has a negative value and the distance on the suction side is represented by a positive value. C is the blade chord length. It can be seen that (1) prediction of pressure coefficient distributions by all turbulence models agree with the test data relative well, except those of the SST model and LCTM (S-J) at downstream of the transition location, (2) prediction of pressure coefficients is insensitive to the near-wall grid resolution, (3) all turbulence models can neither reasonably predict the heat transfer to the wall, nor capture the transition effect on the heat transfer to the wall, (4) refinement of the near-wall grid spacing improve the numerical accuracy of turbulence models in predicting heat transfer to the wall, and (5) the SST model and LCTM are more sensitive to the near-wall grid spacing than the low-Re k-ε and Walters-Leylek models in predicting the heat transfer to the wall. Fig. 23 shows the pressure contours predicted by the laminar flow model, the Walters-Leylek model, and the LCTM (S-J). The axial velocity contours and velocity vectors obtained from those three models are also demonstrated in Fig. 24. The laminar flow result shows flow near separation on the suction side towards the trailing edge, and has a stronger wake region behind the blade trailing edge than those predicted by the Walters-Leylek model and the LCTM (S-J).

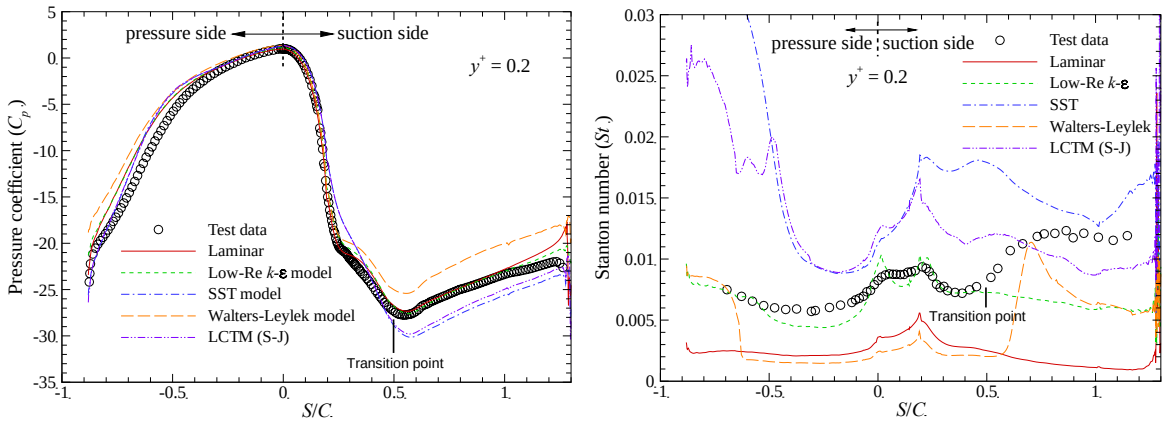

Fig. 20: Comparisons of predicted pressure coefficient and Stanton number distributions along the blade surface (y^+ = 0.2)

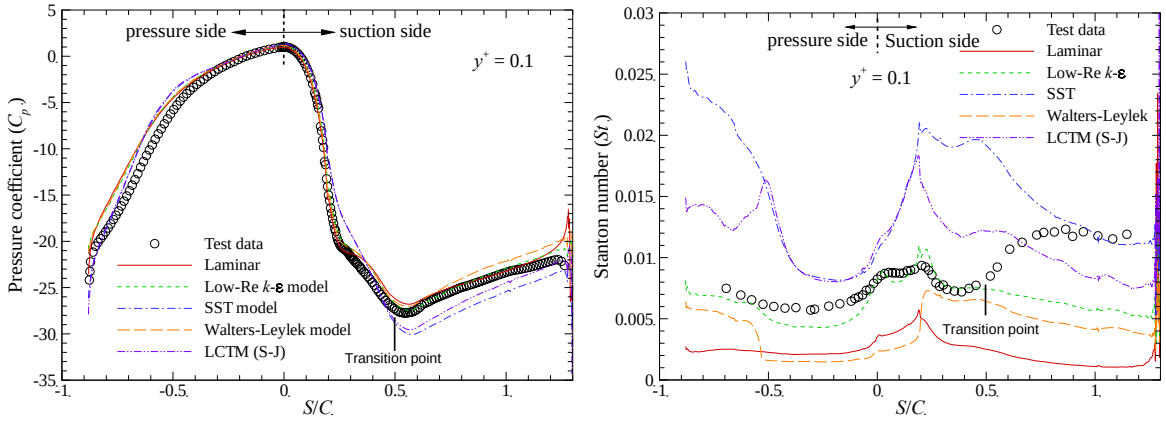

Fig. 21: Comparisons of predicted pressure coefficient and Stanton number distributions along the blade surface (y^+ = 0.1)

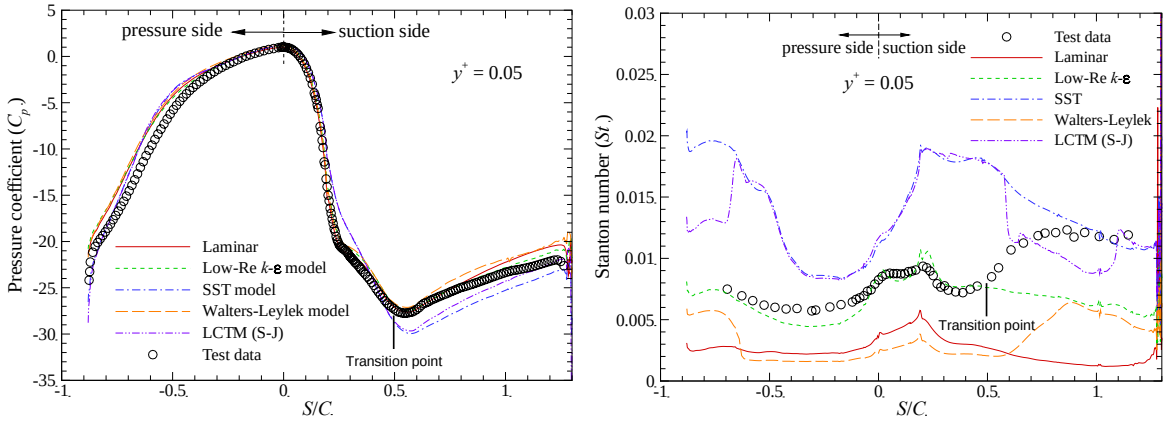

Fig. 22: Comparisons of predicted pressure coefficient and Stanton number distributions along the blade surface (y^+ = 0.05)

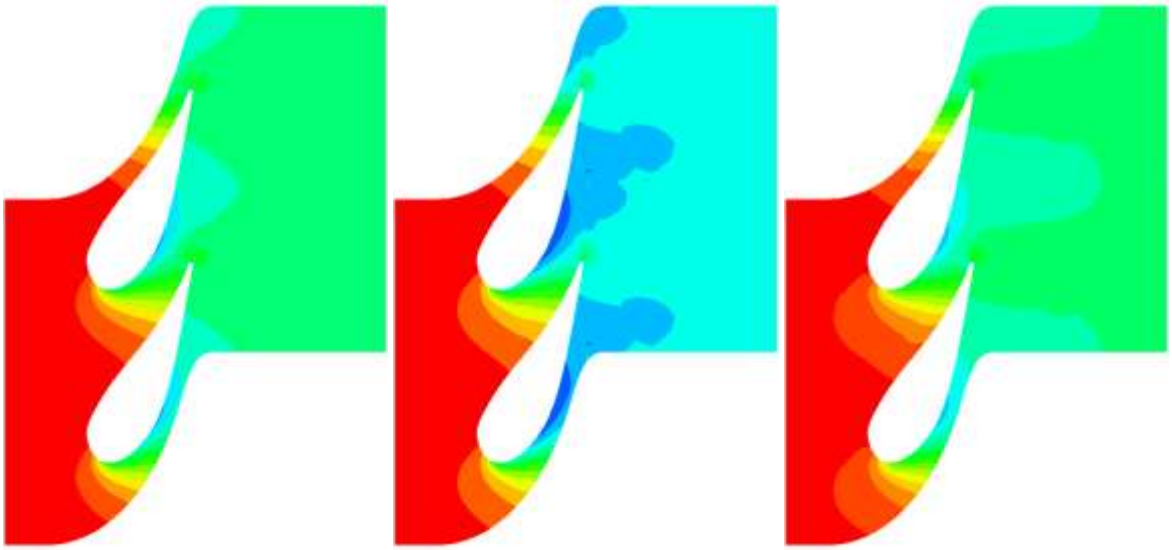

(a) Laminar (b) Walters-Leylek model (c) LCTM (S-J)

Fig. 23: Comparisons of predicted pressure contours (y^+ = 0.05)

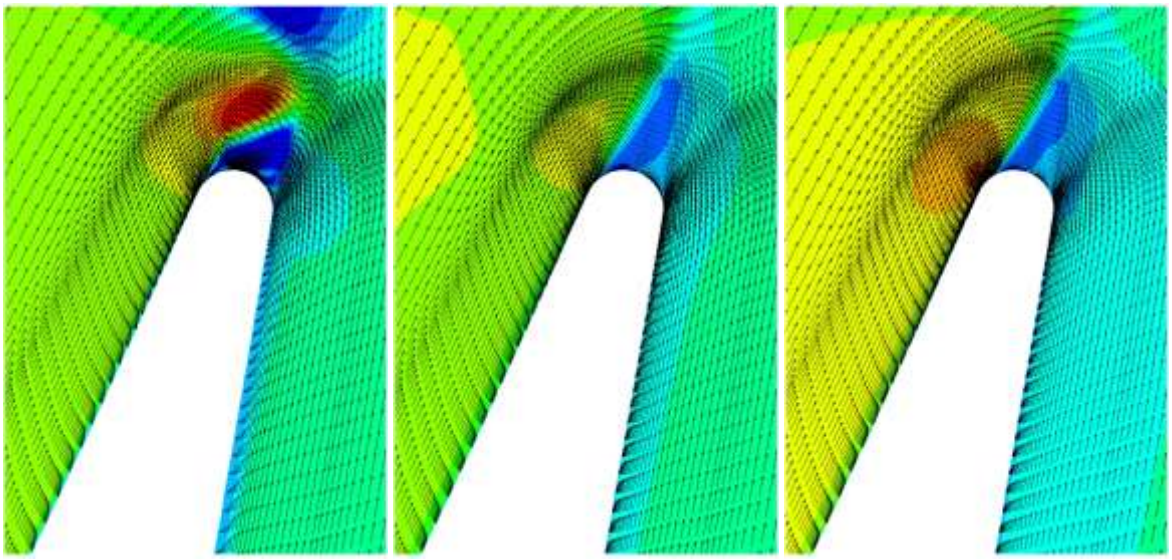

(a) Laminar (b) Walters-Leylek model (c) LCTM (S-J)

Fig. 24: Comparisons of axial velocity contours and velocity vectors near the trailing edge (y^+ = 0.05)

An overset grid system (2 blocks: 241×102, 181×101), shown in Fig. 25, has a near-wall y^+ of 0.1 and is used by the OVERFLOW code with the LCTM (N-L). The pressure coefficient and Stanton number distributions along the blade surface predicted by the LCTM (N-L), implemented in the OVERFLOW code, are compared to the test data and the results of the LCTM (S-J). The comparison is plotted as shown in Fig. 26. It can be seen that the pressure coefficient distributions predicted by the LCTM with N-L correlations agree well with the test data. However, similar to other transition models the LCTM with N-L correlations fail to capture the transition effect on the heat transfer to the wall along the suction surface. Fig. 26 indicates that heat transfer to the wall predicted by the LCTM with both the N-L and S-J correlations follows the trend similar to the test data on the pressure side, but the S-J correlation over-predicts its magnitude while the N-L correlation under-predicts it. On the suction side, the LCTM with both the N-L and S-J correlations predict similar heat transfer to the wall without capturing the transition effect. It should be noted that the pressure gradient correction in the LCTM (N-L) was not turned on in this simulation. Overall, the success of these transition models in predicting wall pressure distribution does not lead to the accuracy in wall heat flux computations. The inaccuracy in predicting the wall heat flux is believed to be caused not only by the transition model itself, but also the order of accuracy in the spatial domain of the numerical algorithms in the employed CFD codes. In this study, second-order accuracy in space was used in the numerical computation for both FDNS and OVERFLOW codes, which may be inadequate. The temperature near the wall is known to vary steeper than the pressure, and thus either much finer mesh or higher-order accuracy in spatial discretization may be used to improve the accuracy of these transition models.

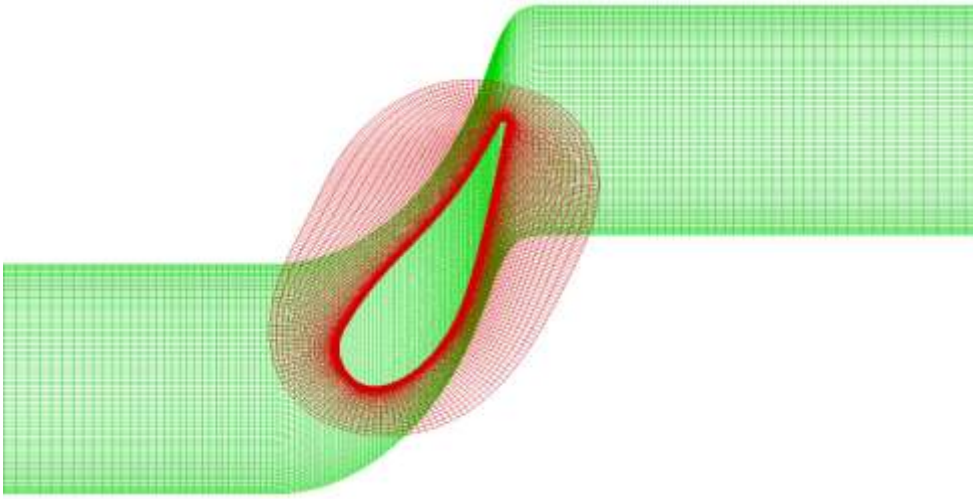

Fig. 25: Overset mesh system for a subsonic flow over a turbine stator cascade

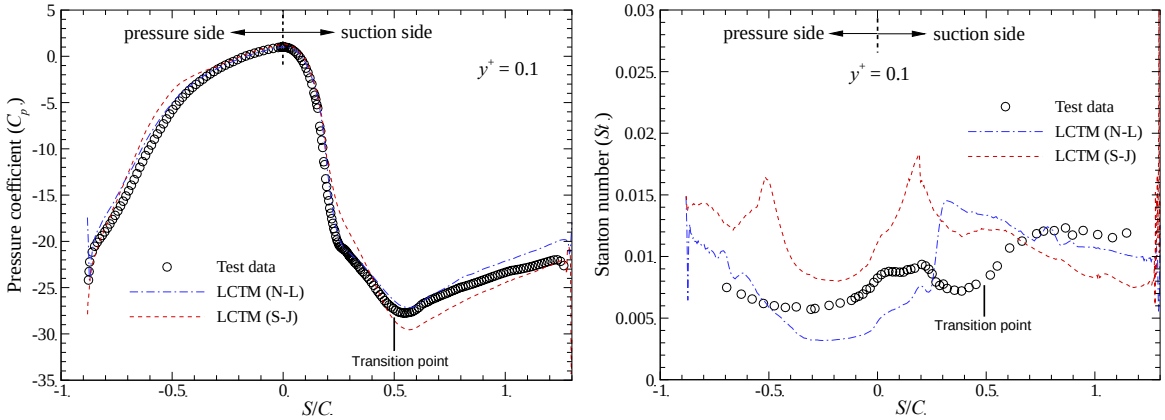

Fig. 26: Comparisons of predicted pressure coefficient and Stanton number distributions along the blade surface (y^+ = 0.1)

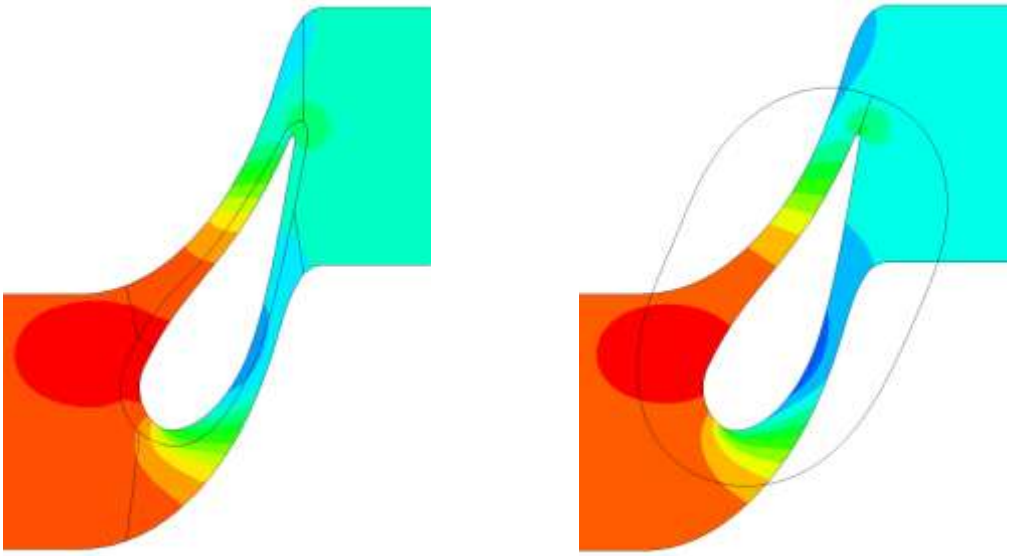

(a) LCTM (S-J) (b) LCTM (N-L)

Fig. 27: Comparisons of predicted pressure contours ($y^+ = 0.1$)

V. CONCLUSIONS AND RECOMMENDATIONS

An extensive literature review of turbulence transition models was conducted, and its result is summarized in this paper. Both the Walters-Leylek model and LCTM were selected for evaluation in this study. The Walters-Leylek model and LCTM (with the S-J correlations) were implemented in the FDNS code, while LCTM with both the S-J and N-L correlations were implemented in the OVERFLOW-2.1 code. The assessment of the Walters-Leylek model and LCTM were performed using three sets of benchmark test cases. For flow over a flat plate (T3 series), the Walters-Leylek model and LCTM were shown to properly account for effects of turbulent transition to different extents. The result shows that both models can capture the onset as well as the region of turbulence transition very well when the upstream turbulence level is high. As the upstream turbulence intensity decreases prediction of the size of the transition region starts to deviate from the test data, and then followed by deviation in the prediction of transition onset location. Neither model can accurately predict both the magnitude and decay of freestream turbulence intensity for all three test cases. In addition, LCTM is shown to be more sensitive to the near-wall grid resolution than the Walters-Leylek model. For the cases in this study performed with OVERFLOW the N-L correlation performs better than the S-J correlation for LCTM. For the case of hypersonic flow over a cylindrical cone, LCTM with the S-J correlation fails to capture the transition effect, whereas, LCTM with the N-J correlation can predict the expected trend for turbulence transition as a function of free stream turbulence level. The Walters-Leylek model requires very fine near-wall grid resolution to capture the transition effect, but fails to predict the location of transition onset correctly. The pressure distribution in the subsonic flow over a stator blade cascade was well predicted by all turbulence models despite none of them properly capture the transition effect. This deficiency is clearly shown in predicting heat transfer to the blade surface, especially on the suction side where turbulence transition occurs. To improve the accuracy of predicting the transition effect on wall heat flux a higher-order accuracy in spatial discretization may be required in addition to the transition model.

Overall, both the Walters-Leylek model and LCTM are shown to have the potential of predicting the location for turbulence transition for some cases. This should enable the eddy-viscosity model based CFD codes to simulate the flow characteristics in the transition region for the class of flow problems validated. However, the range of applicability and validity for both transition models is still questionable. Hence, these transition models need further improvement and validation to improve their accuracy and range of applicability. In addition to the modeling of turbulence transition, research on understanding the underlying physics associated with turbulence transition for different flow regimes/environments using direct numerical simulations has increased its feasibility with the advance of computing power nowadays.

ACKNOWLEDGMENT

This work was made possible through support provided by DoD HPCMP PET activities through Mississippi State University under contract No. GS04T01BFC0060/0072. Inputs from Fred Shope at AEDC, Hugh Thornburg at Mississippi State University, and Roger Kimmel at Wright-Patterson Air Force Base are greatly appreciated.

REFERENCES

[1]. A. M. O. Smith, "Transition, Pressure Gradient and Stability Theory," Douglas Aircraft Co. Rept. ES26388, El Segundo, California, 1956.

[2]. J. L. van Ingen, "A Suggested Semi-empirical Method for the Calculation of the Boundary Layer Transition Region," University of Technology, Department of Aero. Eng., Rep. UTH-74, Delft, 1956.

[3]. M. T. Arthur, and C. J. Atkin, "Transition Modeling for Viscous Flow Prediction," AIAA Paper, AIAA Paper 2006–3052, 2006.

[4]. S. A. McKeel, "Numerical Simulation of the Transition Region in Hypersonic Flow," PhD dissertation, Blacksburg, Virginia, 1996.

[5]. P. Stainback, M. Fisher, and R. Wagner, "Effects of Wind-Tunnel Disturbances on Hypersonic Boundary Transition," AIAA Paper 72–181, 1972.

[6]. M. Holden, and K. Chadwick, "Studies of Laminar, Transitional, and Turbulent Hypersonic Flows Over Curved Compression Surfaces," Tech. Rep. 2610-5, Calspan-UB Research Center, 1994.

[7]. R. Kimmel, "Experimental Transition Zone Lengths in Pressure Gradient in Hypersonic Flow," Symposium on Transitional and Turbulent Compressible Flows (Kral, L. and Zang, T., eds.), Vol. FED 151, 1993, pp. 117-127.

[8]. R. Kimmel, "The Effect of Pressure Gradients on Transition Zone Length in Hypersonic Boundary Layers," Tech. Rep. WL-TR-94-3012, Wright Laboratory, Wright Patterson AFB, 1993.

[9]. E. S. Warren, J. E. Harris, and H. A. Hassan, "Transition Model for High-Speed flow," *AIAA Journal*, Vol. 33, No. 8, 1995, pp. 1391–1397.

[10]. S. Dhawan, and R. Narasimha, "Some Properties of Boundary Layer Flow During Transition from Laminar to Turbulent Motion," *Journal of Fluid Mechanics*, Vol. 3, No. 4, 1958, pp. 418–436.

[11]. D. C. Wilcox, "Turbulence Modeling for CFD," La Canada, CA, DCW Industries, 1992.

[12]. D. C. Wilcox, "Turbulence and Transition Modeling for High-Speed Flows," NASA CR 191473, 1993.

[13]. R. Schmidt, and S. Patankar, "Simulating Boundary Layer Transition with Low-Reynolds Number k-e Turbulence Models: Part 2 - An Approach to Improving the Predictions," *Journal of Turbomachinery*, vol. 113, 1991, pp. 18–26.

[14]. C. Lam, and K. Bremhorst, "A Modified Form of the k-e Model for Predicting Wall Turbulence," ASME *Journal of Fluids Engineering*, Vol. 103, 1981, pp. 456–460.

[15]. D. Arnal, "Three-Dimensional Boundary Layers: Laminar-Turbulent Transition," AGARD-FDP-VKI Special Course on Calcul Des Limites Tridimensionelles Avec Ou Sans Decollement, 1986.

[16]. D. Arnal, "Laminar-Turbulent Transition Problems in Supersonic and Hypersonic Flows," AGARD-FDP-VKI Special Course on Aerothermodynamics of Hypersonic Vehicles, 1988.

[17]. B. Singer, S. Dinavahi, and V. Iyer, "Testing of Transition-Region Models: Test Cases and Data," NASA CR 4371, 1991.

[18]. Singer, B., 1993, "Modeling the Transition Region," NASA CR 4371.

[19]. J. Dey, and R. Narasimha, "An Integral Method for the Calculation of 2D Transitional Boundary Layers," *Journal of Aircraft*, Vol. 27, No.10, 1990, pp.859–865.

[20]. R. Abid, "A Study of Turbulence Models for Prediction of Transitional Boundary Layers," Instability, Transition, and Turbulence (Hussaini, Kumar, and Streett, eds.), Springer-Verlag, 1992.

[21]. C. J. Roy, and F. G. Blottner, "Assessment of One- and Two-Equation Turbulence Models for Hypersonic Transitional Flows," *Journal of Spacecrafts and Rockets*, Vol. 38, No.5, 2001, pp. 313–325.

[22]. P. R. Spalart, and S. R. Allmaras, "A One-Equation Turbulence Model for Aerodynamic Flows," AIAA paper 92–0439, 1992.

[23]. B. S. Baldwin, and T. J. Barth, "A One-Equation Transport Model for High Reynolds Number Wall-Bounded Flows," NASA TM–102847, 1990.

[24]. Y. Nagano, and M. Hishida, "Improved Form of the k-ε Model for Wall Turbulent Shear Flows," *J. of Fluid Eng*., **109**(2), 1987, pp. 156–160.

[25]. F. R. Menter, "Two-Equation Eddy Viscosity Turbulence Models for Engineering Applications," *AIAA J.*, Vol. 32, No. 8, 1994, pp. 1598–1605.

[26]. D. C. Wilcox, *Turbulence Modeling for CFD*, 2nd ed., La Canada, CA, DCW industries, Chap.5, 1998, pp. 119–122 and 227–271.

[27]. X. Xiao, J. R. Edwards, and H. A. Hassan, "Transitional flow over an Elliptic Cone at Mach 8," *Journal of Spacecraft and Rockets*, Vol. 38, No. 6, 2001, pp. 941–945.

[28]. M. V. Mokovin, "Bypass Transition to Turbulence and Research Desiderata," Transition in Turbines, edited by R. W. Graham, NASA CP2386, 1985, pp. 161–204.

[29]. J. L. Papp, and S. M. Dash, "Rapid Engineering Approach to Modeling Hypersonic Laminar-to-Turbulent Transitional Flows," *Journal of Spacecraft and Rockets*, Vol. 42, No. 3, 2005, pp. 467–475.

[30]. R. M. C. So, S. Sarkar, G. Gerodimos, and J. Zhang, "A Dissipation Rate Equation for Low-Reynolds-Number and Near-Wall Turbulence," *Theoretical Computational Fluid Dynamics*, Vol. 9, 1997, pp. 47–63.

[31]. E. W. Waren, and H. A. Hassan, "Alternative to the e^n Method for Determining Onset of Transition," *AIAA Journal*, Vol. 36, No. 1, 1998, pp. 111–113.

[32]. Y. B. Suzen, and P. G. Huang, "An Intermittency Transport Equation for Modeling Flow Transition," AIAA Paper 2000–0287, 2000.

[33]. J. Steelant, and E. Dick, "Modeling of Bypass Transition with Conditioned Navier-Stokes Equations Coupled to an Intermittency Transport Equation," *International Journal for Numerical Methods in Fluids*, Vol. 23, 1996, pp. 193-220.

[34]. J. R. Cho, and M. K. Chung, "A k-e-v Equation Turbulence Model," *Journal of Fluid Mechanics*, vol. 237, 1992, pp. 301–322.

[35]. P. G. Huang, and G. Xiong, "Transition and Turbulence Modeling of Low Pressure Turbine Flows," AIAA Paper, 98–0339, Reno, NV, 1998.

[36]. A. M. Savill, "Some Recent Progress in the Turbulence Modeling of By-pass Transition," *Near-Wall Turbulent Flows*, edited by R.M.C. So, C.G. Speziale and B.E. Launder, Elsevier Science Publishers B.V., 1993, pp. 829–848.

[37]. A. M. Savill, "Further Progress in the Turbulence Modeling of By-pass Transition," *Engineering Turbulence Modeling and Experiments* 2, edited by W. Rodi and F. Martelli, Elsevier Science Publishers B.V., 1993, pp. 583–592.

[38]. D. K. Walters, and J. H. Leylek, "A New Model for Boundary Layer Transition Using a Single-Point RANS Approach," *Journal of Turbomachinery*, Vol. 126, Issue 1, 2004, pp. 193–202.

[39]. R. E. Mayle, and A. Schulz, ''The Path to Predicting Bypass Transition,'' *Journal of Turbomachinery*, Vol. 119, 1997, pp. 405–411.

[40]. R. B. Langtry, and F. R. Menter, "Transition Modeling for General CFD Applications in Aeronautics," AIAA Paper 2005–522, 2005.

[41]. F. R. Menter, R. B. Langtry, S. R. Likki, Y. B. Suzen, P. G. Huang, and S. Volker, "A Correlation-based Transition Model Using Local Variables Part I - Model Formulation," *Journal of Turbomachinery*, Vol. 128, 2006, pp. 413–422.

[42]. K. Lodefier, B. Merci, C. De Langhe, and E. Dick, "Intermittency Based RANS Bypass Transition Modeling," *Progress in Computational Fluid Dynamics*, Vol. 6, Nos. 1/2/3, 2006, pp. 68-78.

[43]. J. Steelant, and E. Dick, "Modeling of Laminar- Turbulent Transition for High Freestream Turbulence," *Journal of Fluids Engineering*, Vol. 123, No. 1, 2001, pp. 22–30.

[44]. Y. Lian, and W. Shyy, "Laminar-Turbulent Transition of a Low Reynolds Number Rigid or Flexible Airfoil," *AIAA Journal*, Vol. 45, No .7, 2007, pp. 1501–1513.

[45]. K. Suluksna, and E. Juntasaro, "Assessment of Intermittency Transport Equations for Modeling Transition in Boundary Layers Subjected to Freestream Turbulence," *International J. of Heat and Fluid Flow*, Vol. 29, 2008, pp. 48–61.

[46]. R. B. Langtry, "A Correlation-based Transition Model Using Local Variables for Unstructured Parallelized CFD Codes," Ph.D. Dissertation, University of Stuttgart, 2006.

[47]. R. H. Nichols, R. W. Tramel, and P. G. Buning, "Solver and Turbulence Model Upgrades to OVERFLOW 2 for Unsteady and High-Speed Applications," AIAA–2006–2824, June 2006.

[48]. D. C. Jespersen, T. H. Pulliam, and P. G. Buning, "Recent Enhancements to OVERFLOW," AIAA–97–0644, Jan. 1997.

[49]. G. C. Cheng, and R. C. Farmer, "Validation of a Practical Dense-Spray Combustion Model for Liquid Rocket Engine Injector Analyses," *AIAA Journal of Propulsion & Power*, Vol. 22, No. 6, 2006, pp. 1373–1381.

[50]. G. C. Cheng, "Programmers and User's Manual for the FDNS-RFV/MPI CFD Code," Mechanical Engineering Department, University of Alabama at Birmingham, 2000.

[51]. Y. S. Chen, "Compressible and Incompressible Flow Computations with a Pressure Based Method," AIAA Paper 89–0286, 1989.

[52]. J. Coupland, 1993, ERCOFTAC Classic Database, http://cfd.me.umist.ac.uk/ercoftac/

[53]. R. W. Radomsky, and K. A. Thole, "Flowfield Measurements for a Highly Turbulent Flow in a Stator Vane Passage," *ASME Journal of Turbomachinery*, Vol. 122, April 2000, pp. 255–262.

[54]. R. W. Radomsky, and K. A. Thole, "Detailed Boundary Layer Measurements on a Turbine Stator Vane at Elevated Freestream Turbulence Levels," *ASME Journal of Turbomachinery*, Vol. 124, Jan. 2002, pp. 107–118.